Cui *et al. Journal of Nanobiotechnology* (2025) 23:301
https://doi.org/10.1186/s12951-025-03376-0

Journal of Nanobiotechnology

RESEARCH Open Access

Lactobacillus acidophilus extracellular vesicles-coated UiO-66-NH_2@siRNA nanoparticles for ulcerative colitis targeted gene therapy and gut microbiota modulation

Chenyang Cui[1], Jiaze Tang[1], Jie Chen[1], Beining Zhang[1], Ruonan Li[1], Qiang Zhang[2], Chunjing Qiu[3], Rongchen Chen[1], Geng Min[1], Zhaowei Sun[1*] and Haibo Weng[1*]

Abstract

Ulcerative colitis (UC) is a complex and chronic inflammatory bowel disease whose pathogenesis involves genetic and environmental factors, which poses a challenge for treatment. Here, we have designed an innovative integrated therapeutic strategy using *Lactobacillus acidophilus* extracellular vesicles (EVs) to encapsulate UiO-66-NH_2 nanoparticles bounded with TNF-α siRNA (EVs@UiO-66-NH_2@siRNA) for UC treatment. This system shows superior affinity to inflammation-related cells due to the *Lactobacillus acidophilus* EVs can maintain immune homeostasis by regulating the secretion of cytokines in vitro. siRNA can specifically target the key inflammatory TNF-α in UC and silence its gene expression, thereby regulating the process of inflammatory response. After oral administration, EVs@UiO-66-NH_2@siRNA demonstrates an accurate delivery of TNF-α siRNA to colonize the colon site and exerts a siRNA therapeutic effect by inhibiting the expression of TNF-α, which alleviates the intestinal inflammation in DSS-induced UC model. Moreover, this system can modulate the types and compositional structures of gut microbiota and metabolites to achieve an anti-inflammatory phenotype, which is helpful for the repair of intestinal homeostasis. We also have proved that UiO-66-NH_2 nanoparticles exhibit a high loading capacity for TNF-α siRNA and good pH responsiveness, improving the potent release of siRNA in colon tissue. Collectively, the EVs@UiO-66-NH_2@siRNA nano-delivery system demonstrate a feasible combination therapeutic strategy for UC through gut microecology modulation, immune regulation and TNF-α siRNA silence, which may provide a potential targeted treatment approach for inflammatory bowel disease.

*Correspondence:
Zhaowei Sun
szw@zzu.edu.cn
Haibo Weng
whb@zzu.edu.cn
[1]School of Life Sciences, Zhengzhou University, Zhengzhou, Henan 450001, China
[2]Department of Critical Care Medicine, The Fifth Affiliated Hospital of Zhengzhou University, Zhengzhou, Henan 450052, China
[3]Henan Key Laboratory of Helicobacter Pylori & Microbiota and Gastrointestinal Cancer, Marshall Medical Research Center, The Fifth Affiliated Hospital of Zhengzhou University, Zhengzhou, Henan 450052, China

Graphical Abstract

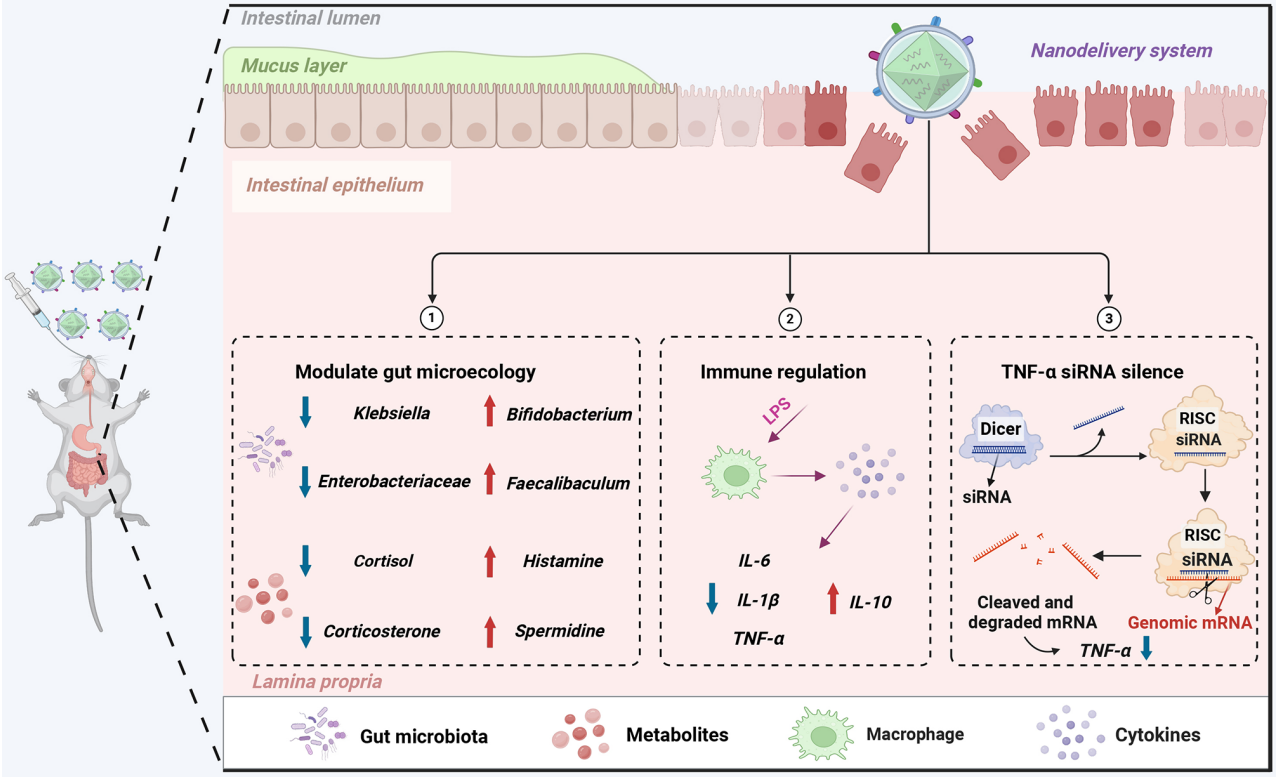

Keywords Ulcerative colitis, *Lactobacillus acidophilus* EVs, TNF-α SiRNA, UiO-66-NH_2, Targeted gene therapy

Introduction

Ulcerative colitis (UC) is a chronic inflammatory bowel disease characterized by complex immune responses and dysbiosis of the gut microbiota [1]. Although current therapeutic drugs such as 5-aminosalicylic acid, corticosteroids, and inhibitors can partly alleviate symptoms, the side effects associated with their long-term use remain a challenge in UC treatment [2]. The dysbiosis of the gut microbiota and abnormalities in metabolism have been closely linked to the pathogenesis of UC [3, 4]. The gut microbiota, as a crucial ecosystem within the organism, can impact immune cell differentiation and activation in immune regulation. In terms of metabolic functions, it plays an important role in various metabolic pathways such as nutrient digestion and absorption [5]. Research has shown that the diversity of gut microbiota in UC patients has reduced, for instance the increase of pathogenic bacteria and the decrease of probiotics, which leads to the deterioration of intestinal mucosal barrier function and disease progression [6, 7]. Furthermore, metabolites serve as important mediators of interaction between the gut microbiota and the host, and changes of their types and levels impact directly the host's metabolic status and immune response [8, 9]. Therefore, methods focused on modulating the gut microbiota and metabolites have gained significant attention and become a research hotpot in UC treatment [10].

Lactobacillus acidophilus, as an important probiotic, has been found to improve the efficacy of UC therapy by regulating the composition of gut microbiota and metabolites [11]. For example, *Lactobacillus acidophilus* could produce beneficial metabolites, such as short-chain fatty acids, which help maintain intestinal mucosal health and moderate organismal metabolism [12]. Moreover, *Lactobacillus acidophilus* has the ability to inhibit the growth of pathogenic bacteria and promote the proliferation of probiotics, remolding the balance of gut microbiota [13]. Some reported also demonstrated that *Lactobacillus acidophilus* can colonize the colon specifically to reduce the levels of pro-inflammatory cytokines (such as TNF-α, IL-6, and IL-1β), and increase the level of anti-inflammatory factors (such as IL-10), thereby promoting intestinal mucosal repair, suppressing the overactive immune system, and alleviating inflammation [14]. However, some limitations still existed in the clinical practice, such as the unsatisfactory effectiveness and inconsistent dosage.

Lactobacillus acidophilus is sensitive and easily deactivated by the pH value and bile salts in gastrointestinal fluid, which result in a low survival rate and unsatisfactory effectiveness [15, 16]. Additionally, individual differences are exhibited in the digestive functional status in UC patients, so, the dosage of *Lactobacillus acidophilus* is varied. This variability makes it complex and challenging to precisely adjust the bacterial dosages in clinical applications [17]. Research has revealed that EVs derived from cells contain proteins, nucleic acids and lipids, which possess properties similar to those of parent cells [18]. Thus, we hypothesize that *Lactobacillus acidophilus* EVs instead of bacterial cells could improve the efficacy of UC treatment.

The imbalance of gut microbiota and abnormal regulation at gene levels play crucial roles in UC pathogenesis [19]. Therefore, RNA interference (RNAi) technology has emerged as a powerful regulation tool. Small interfering RNA (siRNA) as a double-stranded RNA molecule with a length of about 20–25 nucleotides can recognize and bind to the target mRNA in a highly specific manner, which induce endonucleases to cleave the target mRNA for silencing the specific genes [20–22]. This precise gene regulation ability makes siRNA show great potential in UC treatment [23]. The overproduction of tumor necrosis factor-α (TNF-α) stimulates the process of UC pathogenesis, so, inhibiting the function of TNF-α by siRNA maybe break the vicious cycle of inflammatory cascade in intestinal tract and provide a new strategy and direction for UC treatment [24, 25].

In this study, we have prepared a dual-mode UC therapeutic system using *Lactobacillus acidophilus* EVs and TNF-α siRNA drugs. To improve the therapeutic efficiency of siRNA, UiO-66-NH_2 is first synthesized, and then bonded with a large amount of TNF-α siRNA through multivalent interactions to synthesize UiO-66-NH_2@siRNA nanoparticles. UiO-66-NH_2 possesses several advantages over other nanomaterials (liposomes or dendrimers), such as high surface area, tunable pore size, and acid-sensitive properties, which facilitated the efficient loading and release of siRNA in vivo [26–28]. Subsequently, *Lactobacillus acidophilus* EVs are isolated and employed to envelop UiO-66-NH_2@siRNA nanoparticles for the construction of EVs@UiO-66-NH_2@siRNA nano-delivery system (Scheme 1). This system can regulate gut microecology with *Lactobacillus acidophilus* EVs and target TNF-α through TNF-α siRNA for UC treatment through three pathways. (1) Gut microecology modulation: *Lactobacillus acidophilus* EVs are able to modulate the types and compositions of gut microbiota and metabolites by promoting the growth of beneficial bacteria (*Bifidobacterium* and *Faecalibaculum*) and inhibiting the expansion of pathogenic bacteria (*Klebsiella* and *Enterobacteriaceae*) to improve intestinal environmental stability and harmony. (2) Immune regulation: *Lactobacillus acidophilus* EVs can effectively regulate the secretion of inflammatory factors in intestinal cells, reducing the production of pro-inflammatory cytokines (such as IL-6, IL-1β, and TNF-α) and increasing the levels of anti-inflammatory factors (like IL-10). This promotes the repair and regeneration of intestinal mucosa, leading to a reduction in intestinal inflammation. (3) TNF-α siRNA silence: TNF-α siRNA in this system specifically silences the TNF-α gene and reduces their expression level in colonic inflammatory tissues, which decreases the infiltration of inflammatory cells and tissue damage and maintain the stability of the intestinal environment. We have demonstrated that this system is superior in the following ways: (1) UiO-66-NH_2 features with high porosity, large surface area, and acid sensitivity, which can increase the loading amounts of TNF-α siRNA and improve its escape efficiency from lysosomes. (2) Intestinal-site targeting and preferential colonization of *Lactobacillus acidophilus* EVs enables this system to quickly reach the disease-site for boosting the effectiveness of TNF-α siRNA against UC. This nano-delivery system also reduces the off-target side effects and provides a more precise means of treatment. Overall, targeted delivery of TNF-α siRNA to the inflamed site and modulation of the gut microbiota and metabolites using *Lactobacillus acidophilus* EVs-coated UiO-66-NH_2 shows great potential for the UC precise treatment. Given its easy preparation, low cost and good biocompatibility, the developed strategy opens up a new avenue for the advanced delivery of siRNA with probiotic EVs in biomedical applications.

Experimental sections

Chemicals and reagents

Zirconium tetrachloride ($ZrCl_4$, purity ≥ 99%), 2-aminoterephthalic acid (NH_2-BDC, purity ≥ 98%), N, N-dimethylformamide (DMF, purity ≥ 99.5%), and benzoic acid (purity ≥ 99%) were purchased from Sigma-Aldrich (MO, USA). Dextran sulfate sodium (DSS, colitis grade, Mw = 36–50 kDa, purity ≥ 95%) was obtained from MP Biomedicals (CA, USA). The MTT Cell Proliferation and Cytotoxicity Assay Kit was purchased from EnoGene (Nanjing, China). The NaviScript® Rapid PCR Master Mix (601112) was ordered from Synomebio Co., Ltd. (Shanghai, China). The StarLighter HP SYBR Green qPCR Mix was purchased from Foreverstar Biotech (Beijng, China). RNase III (E153) and RNase free water (E132) were ordered from Novoprotein (Shanghai, China). RNA extraction kits was purchased from Beibei Biotechnology Co. Ltd. (Zhengzhou, China). The PCR product purification kits was purchased from Shandong Sparkjade Biotechnology Co., Ltd. (Shandong, China). The Evo M-MLV reverse transcription kits (AG11705) was ordered from ACCURATE BIOTECHNOLOGY (Hunan) Co., Ltd,

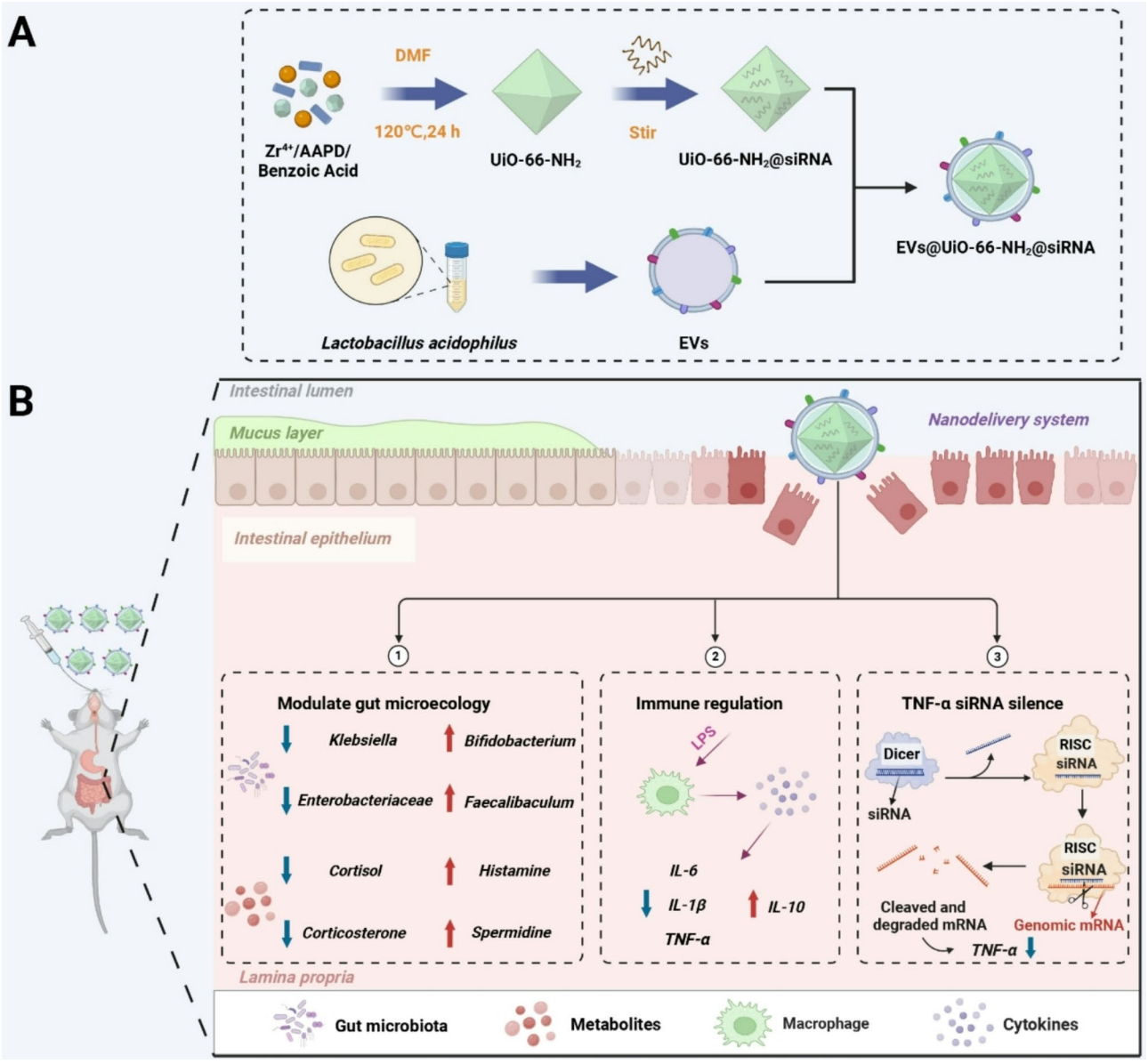

Scheme 1 EVs@UiO-66-NH_2@siRNA nano-delivery system for the treatment of UC. (**A**) Preparation process of EVs@UiO-66-NH_2@siRNA. (**B**) EVs@UiO-66-NH_2@siRNA specifically treat UC

(Changsha, China). The dsDNA quantification kit was bought from Invitrogen (CA, USA). TNF-α siRNA (sense: 5'-GUCUCAGCCUCUUCUCAUUCCUGCT-3', anti-sense: 5'-AGCAGGAAUGAGAAGAGGCUGAG ACAU-3'), carboxy fluorescein (FAM)-labeled siRNA, as well as primers for TNF-α, IL-6, IL-1β and IL-10 were synthesized by Beijing Tsingke Biotech Co., Ltd. (Beijing, China). Cy5.5-labeled-siRNA was synthesized from Bioligo Biotechnology (Shanghai) Co., Ltd. (Shanghai, China). MRS medium, BCA protein concentration assay kit, RPMI 1640 medium, 4% paraformaldehyde (purity ≥ 99%) and ELISA kits for IL-1β (SEKM-0002) cytokines were purchased from Solarbio Science & Technology Co., Ltd. (Beijing, China). The ELISA kits for TNF-α (EMC102a.96) was ordered from Neobioscience Technology Co, Ltd. 200-mesh copper grids and uranyl acetate (purity ≥ 99%) were obtained from Zhongjingkeyi Technology Co., Ltd. (Beijing, China). FBS was ordered from Inner Mongolia Wanrui Biotechnology Co.,Ltd. (Neimenggu, China). DAPI (purity ≥ 98%) and Lyso-Tracker (purity ≥ 95%) were provided by Beyotime Biotechnology (Shanghai, China). ELISA assay kits for IL-6 (JL20268) cytokines was obtained from Jianglai biology (Shanghai, China). The IL-10 ELISA kits (CSB-E04594m-IS) was obtained from Signalway Antibody (Nanjing, China). The myeloperoxidase (MPO) assay kit was

purchased from Nanjing Jiancheng Bioengineering Institute (Nanjing, China). The Kryogene™ cell preservation solution was obtained from Milecell Biological Science & Technology Co., Ltd. (Shanghai, China). The PCR tubes, 15 mL centrifuge tubes and 50 mL centrifuge tubes were purchased from Hangzhou Agen biotechnology limited. (Hangzhou, China). The SDS-PAGE Protein Loading Buffer (5X, P011) was obtained from GenulN (Hefei, China). Agarose was purchased from Coolaber Science & Technology (Beijing, China). Small molecular weight Tricine prefabricated glue (TR10165Gel) obtained from Smartlifesciences (Changzhou, China). The color prestain protein Marker (M323) was purchased from Applied Biological Materials Inc. (abm).

Preparation of UiO-66-NH_2 nanoparticles

UiO-66-NH_2 was prepared based on literature with slight modifications [29, 30]. Firstly, 110 mg of NH_2-BDC, 1.9 g of terephthalic acid, and 120 mg of $ZrCl_4$ were added to 10 mL of DMF, and sonicated for 5 min until completely dissolved. Subsequently, the well-mixed solution was transferred to a 100 mL high-pressure reaction vessel, and placed in an oven at 120 °C for 24 h. After the reaction, the vessel was allowed to cool naturally to room temperature, and the solution inside was collected. The nanoparticles were washed three times with ethanol at 8000 rpm for 10 min. Finally, the washed precipitate was placed in a vacuum drying oven at 65 °C for 12 h, and the UiO-66-NH_2 nanoparticles were collected.

Extraction and purification of *Lactobacillus acidophilus* EVs

Lactobacillus acidophilus (strain number: 1.1878) were acquired from the China General Microbiological Culture Collection Center (Beijing, China), and preserved at -80 °C. Then, it was streaked on solid MRS culture medium, and incubated at 37 °C for resuscitation. After 48 h of cultivation, a single colony was picked and cultured in 4 mL of liquid MRS culture medium, at 37 °C for 24 h. Subsequently, it was inoculated into 400 mL of liquid MRS culture medium and for amplification culture. When the OD600 reached 0.8, the bacterial liquid was centrifuged and collected at 4 °C and 100,000 g for 30 min, followed by filtration through a 0.22 μm filter (CL-SA1-104338, STEEMA, Stronger Science) to remove bacterial cell debris and protein aggregates. The supernatant was then centrifuged at 4 °C and 100,000 g for 1 h, and the precipitate was retained. After washing with PBS solution, the *Lactobacillus acidophilus* EVs were collected, re-suspended in 1 mL PBS solution, and stored at -80 °C for future use.

Preparation of UiO-66-NH_2@siRNA

The UiO-66-NH_2 nanoparticles (1 mg) were mixed with TNF-α siRNA (500 nM) and dissolved in 4 mL of DEPC water. The mixture was stirred at room temperature for 24 h. Subsequently, the solution was centrifuged at 8000 rpm for 10 min, and the precipitate was washed 3 times with DEPC water. The washed samples were then placed in a vacuum drying oven at 65 °C for 12 h to obtain UiO-66-NH_2@siRNA nanoparticles.

Preparation of EVs@UiO-66-NH_2@siRNA

The UiO-66-NH_2@siRNA nanoparticles (1 mg/mL) and *Lactobacillus acidophilus* EVs (0.5 mg/mL, BCA protein concentration) were mixed, sonicated for 30 min, and then passed through porous polycarbonate membranes with pore sizes of 800 nm, 400 nm, 200 nm, and 100 nm (Millipore, Germany) with a liposome extruder (Morgec Machinery, Shanghai, China). The resulting solution was centrifuged at 12,000 rpm for 5 min, and the precipitate was collected. The EVs@UiO-66-NH_2@siRNA nanoparticles were resuspended in PBS and stored at 4 °C for use.

Characterization of nanoparticles

The morphology characteristics of EVs, UiO-66-NH_2, UiO-66-NH_2@siRNA, and EVs@UiO-66-NH_2@siRNA nanoparticles were observed using a transmission electron microscope (Hitachi, Japan). TEM Mapping analysis was also conducted on EVs@UiO-66-NH_2@siRNA. The crystal structures of UiO-66-NH_2 and UiO-66-NH_2@siRNA nanoparticles were analyzed using an X-ray diffractometer (XRD) (Bruker, Germany). The specific surface areas of UiO-66-NH_2 and UiO-66-NH_2@siRNA nanoparticles were determined using the Brunauer-Emmet-Teller (BET) method (Micromeritics, USA). Particle size and zeta potential analysis of EVs, UiO-66-NH_2, UiO-66-NH_2@siRNA, and EVs@UiO-66-NH_2@siRNA nanoparticles were performed using a Malvern particle size analyzer (Mastersizer 2000, UK). The encapsulation efficiency and release rate of siRNA in UiO-66-NH_2 were tested using a microplate reader (BioTek Synergy Mx, USA). The stability of EVs@UiO-66-NH_2@siRNA nanoparticles in RNase and serum was detected using agarose gel electrophoresis. The coating of EVs on UiO-66-NH_2@siRNA nanoparticles was verified using SDS-PAGE.

Cell line and cell culture

The RAW264.7 and HT-29 cells were obtained from the ProMab Biotechnologies Inc (Hunan, China). The cells were cultured in RPMI 1640 medium (BaiDi Biotechnology Co., Ltd. (BDBIO)) supplemented with 10% fetal bovine serum (FBS), penicillin (100 U/mL), and streptomycin (100 μg/mL) at 37 °C in a 5% CO_2 humidified incubator. The medium was changed every 2–3 days, and the cells were passaged when reaching 90% confluence. After the cells were fully grown, the cells were collected in a cryopreservation tube (SAINING Biotechnology) and cryopreserved in liquid nitrogen.

Cell internalization

The RAW264.7 and HT-29 cells were divided into UiO-66-NH_2@FAM-siRNA group and EVs@UiO-66-NH_2@FAM-siRNA group, and the input concentration of FAM-siRNA was 0.5 nmol. Each group was seeded with 4×10^4 cells and cultured for 3 h, 7 h, and 12 h in laser confocal culture dishes (NEST Biotechnology, Wuxi, China). After being washed, the cells were transferred into fresh culture medium containing LysoTracker and incubated at 37 °C for 30 min. The cells were stained with DAPI at 37 °C for 30 min and washed with PBS buffer. Fluorescence images were examined under a 63 × oil mirror lens using a laser confocal microscope (Leica, Germany). ImageJ software was used for quantitative analysis of the average fluorescence intensity of the images.

Flow cytometry

RAW264.7 and HT-29 cells were divided into two groups: UiO-66-NH_2@FAM-siRNA and EVs@UiO-66-NH_2@FAM-siRNA. Cells from each group were seeded in 6-well plates (PakGent Bioscience (Suzhou) Co., Ltd.) at a density of 4×10^4 cells per well. After overnight cultivation, the nanoparticles mentioned above were added and co-incubated with the cells for 3 h, 7 h, and 12 h, with an input concentration of 0.5 nmol FAM-siRNA for each. Then, the cells were washed with PBS to remove unbound siRNA, and digested with trypsin to ensure complete detachment from the culture plate. The resulting cells were washed and collected by centrifugation at 1500 rpm for 5 min. A total of 100 μL of the cell suspension (approximately 10,000 cells) was transferred to a flow cytometry tube (BD, USA) for analysis. The FongCyte™ flow cytometer (Challenbio, Beijing, China) was used to assess the fluorescence intensity utilizing the FITC channel (excitation wavelength at 488 nm, emission wavelength at 525 nm). Flow cytometry data were processed and analyzed using FlowJo V10 software.

Cell vitality

3-(4,5-Dimethylthiazol-2-yl)-2,5-diphenyltetrazolium bromide (MTT) method was used to detect the cell viability [31, 32]. RAW264.7 and HT-29 cells were divided into siRNA group, UiO-66-NH_2 group, EVs group, EVs@UiO-66-NH_2 group, UiO-66-NH_2@siRNA group, and EVs@UiO-66-NH_2@siRNA group. The input concentration of siRNA was 0.1 nmol. Each group was seeded with a quantity of 3×10^3 cells in a 96-well plate (KIRGEN) and co-cultured for 6 h, 12 h, and 24 h. Subsequently, 20 uL of MTT was added to each well and further cultured for 4 h, and the cell viability was determined using an enzyme immunoassay reader at the absorbance of 490 nm.

Induction and treatment of mouse colitis model

All animal procedures and experiments were approved by the Animal Ethics Committee of Zhengzhou University. Six to eight-week-old C57BL/6 female mice were purchased from Beijing Vital River Laboratory Animal Technology Co., Ltd. After a week of acclimatization through normal feeding, the mice were randomly divided into 7 groups: healthy control group, siRNA group, UiO-66-NH_2 group, EVs group, EVs@UiO-66-NH_2 group, UiO-66-NH_2@siRNA group, and EVs@UiO-66-NH_2@siRNA group. Each group contains 5 mice. Colitis models were established by feeding water containing 3% DSS for seven consecutive days. Subsequently, the mice were orally gavaged for 5 consecutive days with a dose of 200 nmol siRNA per mouse. The mice's weight changes were recorded daily. On the 13th day, the mice were euthanized, and the colon as well as organs such as the heart, liver, spleen, lungs, and kidneys were collected. The colon length was measured, and the spleen weight was recorded. All tissues were cleaned with PBS and subjected to H&E and Tunel staining analysis.

Fluorescence imaging analysis in vivo

Cy5.5-labelled siRNA (Cy5.5-siRNA) was used to investigate the distribution of nanoparticles in the gastrointestinal tract. To ensure the reliability and reproducibility of the experiments, healthy adult mice were randomly assigned to three groups: Cy5.5-siRNA, UiO-66-NH_2@Cy5.5-siRNA, and EVs@UiO-66-NH_2@Cy5.5-siRNA, with three mice per group. All mice were acclimated and housed to ensure their optimal health. During the administration phase, each mouse received an oral dose of 800 μL of the nanoparticle solution, with each containing 2 nmol of siRNA. Following administration, the mice were anesthetized with a small animal anesthetic (Beijing Zhongshi Dichuang Technology Development Co., Ltd) at designated time points (0 h, 2 h, 4 h, 6 h, 12 h and 24 h) before euthanasia. Immediately after euthanasia, various tissues and organs of interest, including the intestine, heart, lungs, liver, spleen, and kidneys, were rapidly excised and observed using the IVIS imaging system (excitation wavelength at 675 nm, emission wavelength at 694 nm) (Perkin Elmer, Mass, USA). Image software was used to quantitative analyze the distribution of siRNA.

Enzyme-Linked immunosorbent assay (ELISA)

To detect cytokines in the cell culture supernatant, RAW264.7 and HT-29 cells were seeded at a density of 4×10^4 cells per well in a 96-well plate and cultured overnight. After overnight, the cells were further cultured for 12 h with fresh culture medium containing LPS (150 ng/mL). Subsequently, siRNA, UiO-66-NH_2, EVs, EVs@UiO-66-NH_2, UiO-66-NH_2@siRNA, and EVs@UiO-66-NH_2@siRNA were individually added to the cells, with siRNA at a concentration of 0.1 nmol. The cells were then cultured for another 12 h. The cell culture supernatant was collected by centrifugation at 12,000 rpm. To

detect cytokines in colonic tissues, the colonic tissues were homogenized and the supernatant was collected after centrifugation at 12,000 rpm for 15 min. According to the manufacturer's instructions, the levels of TNF-α, IL-6, IL-1β, and IL-10 in the cell culture supernatant and colonic tissue supernatant were measured using an ELISA assay kit.

Real-time fluorescence quantitative polymerase chain reaction (RT-qPCR)

Total RNA was extracted from the colon tissues of the treated mice, and reversely transcribed into cDNA using a reverse transcription kit. Subsequently, a fluorescence quantitative PCR kit was used to detect the mRNA levels of TNF-α, IL-6, IL-1β, and IL-10. The primer sequences for qPCR were provided in Table S1.

Myeloperoxidase (MPO) analysis

Colon tissue of the treated mice was homogenized and centrifuged at 2000 rpm for 15 min at 4℃ using a low-temperature centrifuge. The supernatant was collected and analyzed using a myeloperoxidase assay kit according to the literature [33].

In vivo safety analysis

The female C57BL/6 mice at age of 6–8 week was randomly assigned into control group and EVs@UiO-66-NH_2@siRNA group, with 3 mice in each group. The mice were orally gavaged with PBS and EVs@UiO-66-NH_2@siRNA nanoparticles containing 6 nmol of siRNA. After 24 h, the mice were euthanized, and the important organs were collected and H&E and fluorescence TUNEL staining were performed. The blood samples were centrifuged at 3000 rpm for 20 min at 4 °C, and the supernatant was carefully collected. Subsequently, the levels of aspartate aminotransferase (AST) and alanine aminotransferase (ALT) were determined using kits (KTB1410 and KTB1420, Abbkine, Wuhan, China) according to the manufacturer's provided instructions.

16 S rRNA gene amplicon sequencing

16s rRNA sequencing and analysis was performed at Wuhan ProNets TestingTechnology Co., Ltd (Wuhan, China). PCR amplification of the bacterial 16 S rRNA genes V3–V4 region was performed using the forward primer 338 F (5'-ACTCCTACGGGAGGCAGCA-3') and the reverse primer 806 R (5'-GGACTACHVGGGTWTCTAAT-3'). Sample-specific 7 bp barcodes were incorporated into the primers for multiplex sequencing. The PCR components included 5 μL of buffer (5×), 0.25 μL of fast pfu DNA Polymerase (5U/μL), 2 μL (2.5 mM) of dNTPs, 1 μL (10 μM) of forward and 1 μL (10 μM) of reverse primer, 1 μL of DNA Template, and 14.75 mL of ddH_2O. Thermal cycling involved initial denaturation at 98 °C for 5 min, followed by 25 cycles consisting of denaturation at 98 °C for 30 s, annealing at 53 °C for 30 s, and extension at 72 °C for 45 s, with a final extension of 5 min at 72 °C. The purified PCR amplicons were obtained using Vazyme VAHTSTM DNA Clean Beads and quantified using the Quant-iT PicoGreen dsDNA Assay Kit (Invitrogen, Carlsbad, CA, USA). Following individual quantification, the amplicons were pooled in equal amounts, and pair-end 2 × 250 bp sequences was carried out using the Illlumina NovaSeq platform with NovaSeq 6000 SP Reagent Kit (500 cycles) at Shanghai Personal Biotechnology Co., Ltd (Shanghai, China). The α diversity index was characterized by the Chao1 index, Shannon index, and Simpson index. The β diversity analysis was conducted using principal coordinate analysis (PCoA) based on unweighted UniFrac distance matrix.

Nontargeted metabolomics sequencing and analysis

Metabolomic sequencing and analysis were conducted at Shanghai Personal Biotechnology Co., Ltd (Shanghai, China). Metabolites were extracted from mice fecal samples of different groups and analyzed using LC-MS. The pheatmap packages in R (V1.0.12) and ggplot2 (V3.4.1) were used to cluster the abundance values of the metabolites, and bidirectional clustering of the samples and metabolites was performed. A volcano plot was generated to display the abundance of metabolites in the across samples. Differential metabolite abundance values were further subjected to cluster analysis, heatmap plotting, and trend analysis using R. Differential substances were subjected to KEGG enrichment analysis using clusterProfiler (V4.6.0) to obtain significant enrichment information regarding metabolic pathways.

Statistical analysis

Statistical analyses were performed using GraphPad Prism 8.0 and Origin 2021 software. The data were presented as the mean ± standard deviations with three independent tests. One-way analysis of variance (ANOVA) and *t*-tests were used to verify the significant differences between the experimental and control groups, with significance levels denoted by $^{*}P < 0.05$, $^{**}P < 0.01$, and $^{***}P < 0.001$.

Results and discussion

Characterization of EVs@UiO-66-NH_2@siRNA

Empty EVs appeared spherical or cup-shaped under transmission electron microscopy (TEM), while UiO-66-NH_2 and UiO-66-NH_2@siRNA nanoparticles exhibited uniform octahedral shapes. The EVs@UiO-66-NH_2@siRNA nanoparticles displayed a uniformly coated core-shell structure, indicating successful coating of *Lactobacillus acidophilus* EVs onto the surface of UiO-66-NH_2@siRNA nanoparticles (Fig. 1A). TEM energy dispersive

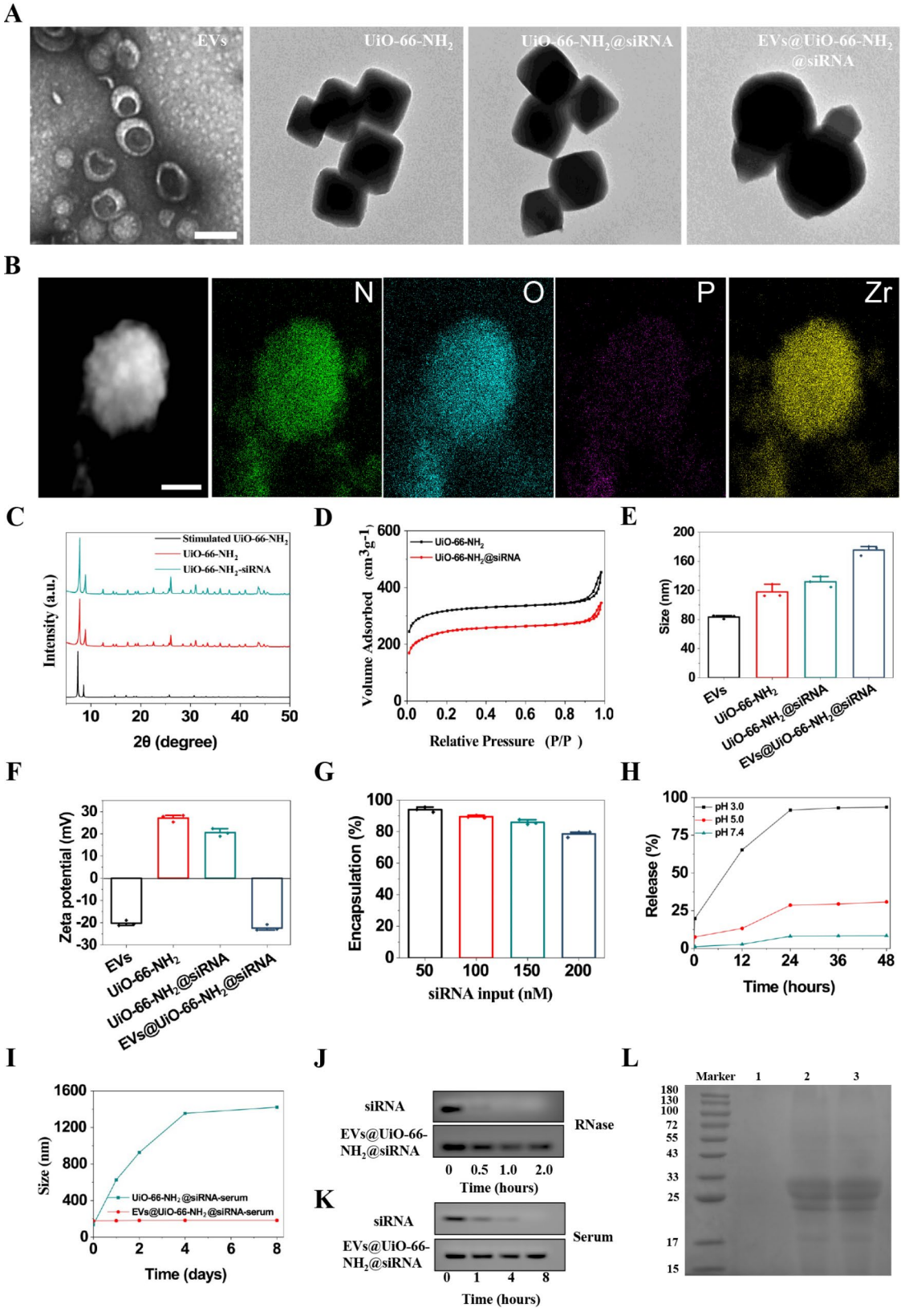

Fig. 1 (See legend on next page.)

(See figure on previous page.)

Fig. 1 Preparation and characterization of EVs@UiO-66-NH_2@siRNA. (**A**) Representative TEM images (scale = 100 nm) of EVs, UiO-66-NH_2, UiO-66-NH_2@siRNA, and EVs@UiO-66-NH_2@siRNA. (**B**) HAADF-STEM image of EVs@UiO-66-NH_2@siRNA and elemental mapping of N, O, P, and Zr (Scale bar = 100 nm). (**C**) XRD spectra of UiO-66-NH_2 and UiO-66-NH_2@siRNA. (**D**) N_2 adsorption-desorption isotherms of UiO-66-NH_2 and UiO-66-NH_2@siRNA. (**E** and **F**) Size and zeta potential of EVs, UiO-66-NH_2, UiO-66-NH_2@siRNA, and EVs@UiO-66-NH_2@siRNA ($n = 3$). (**G**) Encapsulation efficiency of siRNA in EVs@UiO-66-NH_2@siRNA ($n = 3$). (**H**) Time-dependent release of siRNA from EVs@UiO-66-NH_2@siRNA at pH 3.0, pH 5.0, and pH 7.4 ($n = 3$). (**I**) Stability of UiO-66-NH_2@siRNA and EVs@UiO-66-NH_2@siRNA in serum ($n = 3$). (**J** and **K**) Degradation profiles over time of siRNA and EVs@UiO-66-NH_2@siRNA in RNase and serum. (**L**) SDS-PAGE protein analysis of UiO-66-NH_2, EVs, and EVs@UiO-66-NH_2@siRNA (1: UiO-66-NH_2, 2: EVs, 3: EVs@UiO-66-NH_2@siRNA)

X-ray spectroscopy (EDS) elemental mapping confirmed the presence of N, O, P, and Zr elements in the nanoparticles, indicating the presence of siRNA (Fig. 1B). X-ray diffraction patterns revealed highly crystalline structures for UiO-66-NH_2 and UiO-66-NH_2@siRNA nanoparticles, with similar characteristic diffraction peaks, suggesting minimal impact on UiO-66-NH_2 crystallinity after siRNA loading (Fig. 1C). Both UiO-66-NH_2 and UiO-66-NH_2@siRNA nanoparticles exhibited typical Type I isotherms characteristic of microporous materials (Fig. 1D) [34]. The surface area of UiO-66-NH_2 was 1036.15 $m^2\ g^{-1}$ with a pore volume of 0.65 $cm^3 g^{-1}$, whereas UiO-66-NH_2@siRNA had a specific surface area of 916.36 $m^2\ g^{-1}$ and a pore volume of 0.50 $cm^3 g^{-1}$, indicating a decrease in specific surface area and pore volume for UiO-66-NH_2@siRNA due to siRNA occupation within the nanoparticles (Table S2). Dynamic light scattering (DLS) showed EVs to be 83.54 nm in size, UiO-66-NH_2 to be 117.94 nm, but the size of UiO-66-NH_2@siRNA increased to 131.98 nm after siRNA loading. Following EV coating, EVs@UiO-66-NH_2@siRNA size further increased to 175.51 nm (Fig. 1E). Zeta potential measurements revealed a decrease in potential from 27.15 mV to 20.55 mV for UiO-66-NH_2 after loading with negatively charged siRNA. After EV coating, the potential for EVs@UiO-66-NH_2@siRNA decreased to -22.35 mV, like empty EVs which showed – 20.29 mV (Fig. 1F). Additionally, the stability of UiO-66-NH_2@siRNA and EVs@UiO-66-NH_2@siRNA nanoparticles in serum were also explored by measuring the zeta potential overtime. The results showed that the zeta potential of EVs@UiO-66-NH_2@siRNA nanoparticles remained constant throughout 8 days, while the zeta potential of UiO-66-NH_2@siRNA nanoparticles decreased from 20.55 mV to -15.03 mV in 1 day (Fig. S1). These findings suggest that EVs shielding protect UiO-66-NH_2@siRNA nanoparticles form adsorbing serum proteins to form protein coronas, exhibiting good stability under physiological conditions [35]. These changes in size and surface charge confirm the loading of siRNA into nanoparticles and the coating of EVs onto the nanoparticle surface.

The encapsulation efficiency of UiO-66-NH_2 for siRNA was tested using FAM-labeled siRNA (FAM-siRNA). Seen in Fig. 1G, as the input siRNA concentrations increased from 50 nM to 200 nM, the siRNA loading efficiency of UiO-66-NH_2 decreased, with the total loading capacity being highest with 200 nM siRNA. This efficient siRNA loading capability exhibited by UiO-66-NH_2 is consistent with literature reports which showed that oligonucleotides can be adsorbed onto UiO-66-NH_2 through multivalent interactions [36]. We then tested the release of siRNA from EVs@UiO-66-NH_2@siRNA nanoparticles in PBS at different pH levels to determine whether the nanoparticles would degrade within acidic lysosomes. At pH 7.4, a small amount of siRNA was released from the EVs@UiO-66-NH_2@siRNA nanoparticles. Release increased slightly at pH 5.0 and escalated as the acidity intensified; at pH 3.0, over 90% of siRNA was released within 24 h (Fig. 1H). This result suggests that nanoparticles can protect siRNA until they are taken up by cells, where the acidic environment of the lysosomes will degrade the nanoparticles, releasing the siRNA effectively [37]. To assess nanoparticle stability under physiological conditions, we stored UiO-66-NH_2@siRNA and EVs@UiO-66-NH_2@siRNA nanoparticles in serum. As seen in Fig. 1I, the size of UiO-66-NH_2@siRNA nanoparticles reached 1 μm from 134.92 nm over the course of 3 days, whereas the size of EVs@UiO-66-NH_2@siRNA nanoparticles remained almost unchanged over 8 days, indicating that EVs enhance the stability of UiO-66-NH_2@siRNA nanoparticles under physiological conditions (Fig. 1I) [38].

We then examined the role of nanoparticles in preserving siRNA integrity in the presence of RNase and serum. The results showed that siRNA could only exist for 0.5 h in RNase and 4 h in serum before complete degradation. By contrast, little siRNA degradation was observed in EVs@UiO-66-NH_2@siRNA nanoparticles (Fig. 1J, K). This indicates that EVs@UiO-66-NH_2 nanoparticles enhance the stability of siRNA due to the combined protection of the MOF scaffold and EVs [39, 40]. Furthermore, when detecting membrane proteins using polyacrylamide gel electrophoresis, we found that EVs@UiO-66-NH_2@siRNA and EVs exhibited similar protein compositions (Fig. 1L), suggesting that EVs were coated onto the surface of EVs@UiO-66-NH_2 nanoparticles. In conclusion, these results confirm the successful preparation of UiO-66-NH_2 nanoparticles encapsulated with siRNA wrapped in *Lactobacillus acidophilus* EVs.

Cellular internalization of EVs@UiO-66-NH_2@siRNA

The absorption of membrane-modified and unmodified nanoparticles by RAW264.7 and HT-29 cells was examined by encapsulating FAM fluorescence-labeled siRNA

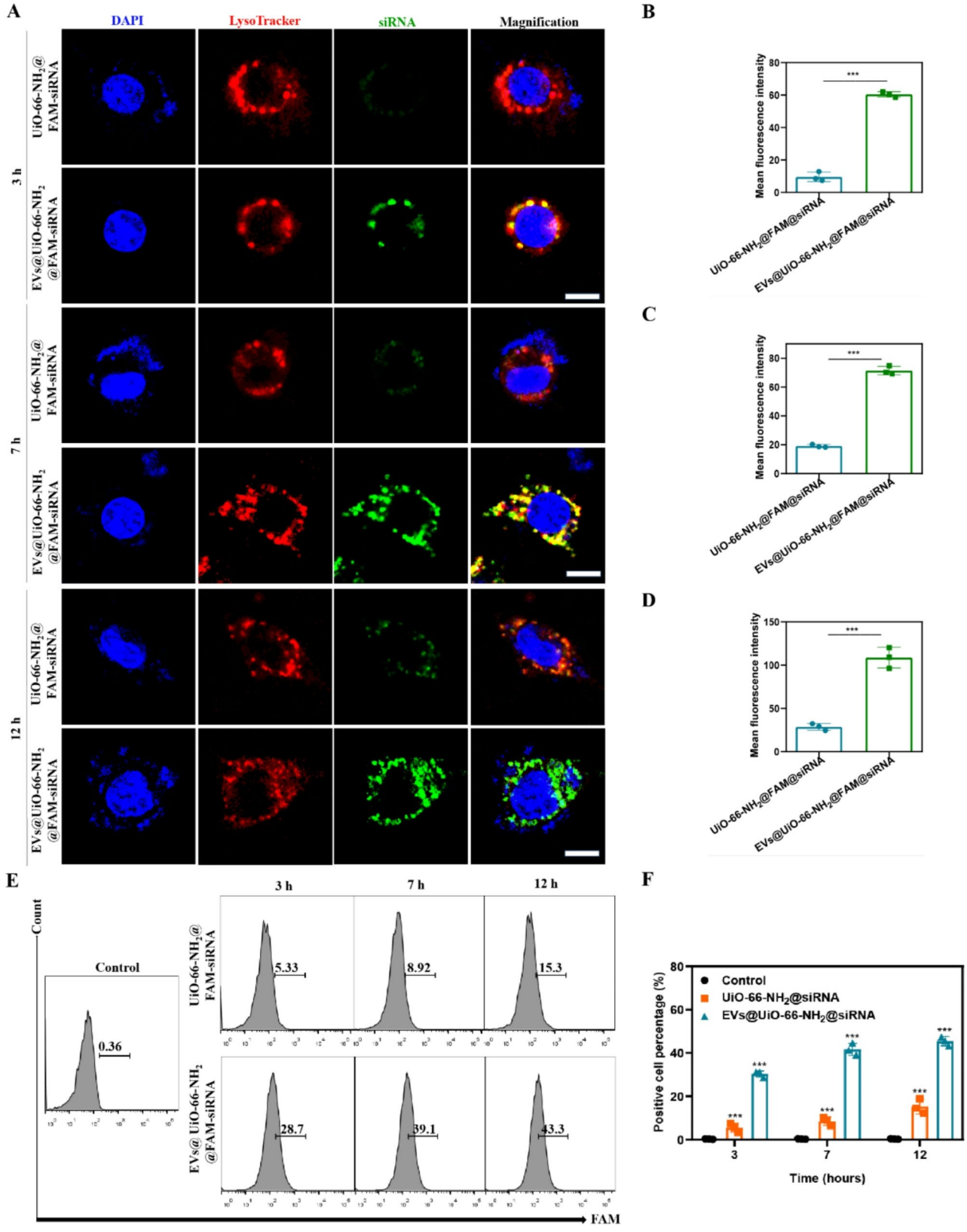

Fig. 2 (See legend on next page.)

(See figure on previous page.)

Fig. 2 Cellular internalization of EVs@UiO-66-NH_2@siRNA. (**A**-**D**) Laser confocal images and green fluorescence quantification of single RAW264.7 cells after co-incubation with UiO-66-NH_2@siRNA and EVs@UiO-66-NH_2@siRNA for 3 h, 7 h, and 12 h. Scale bar = 4.35 μm. The blue channel shows the cell nuclei labeled with DAPI. The red channel shows lysosomes labeled with Lyso-Tracker. The green channel displays siRNA labeled with FAM. (**E** and **F**) Quantitative analysis of green fluorescence in RAW264.7 cells after co-incubation with UiO-66-NH_2@siRNA and EVs@UiO-66-NH_2@siRNA for 3 h, 7 h, and 12 h using flow cytometry ($n = 3$). Data are presented as mean ± SD. *** $P < 0.001$

(FAM-siRNA) in UiO-66-NH_2 and EVs@UiO-66-NH_2, resulting in UiO-66-NH_2@FAM-siRNA and EVs@UiO-66-NH_2@FAM-siRNA. These two types of nanoparticles were co-incubated with RAW264.7 and HT-29 cells for 3 h, 7 h, and 12 h, and cellular internalization and localization were observed using laser confocal microscopy to visualize green fluorescence (Fig. 2A-D, Fig. S2 A-D and Fig. S3 A-D). After 3 h of co-incubation, more green fluorescence (siRNA) was observed in the EVs@UiO-66-NH_2@FAM-siRNA group compared to the UiO-66-NH_2@FAM-siRNA group, indicating that membrane modification with EVs enhanced the absorption of nanoparticles by RAW264.7 and HT-29 cells, highlighting the known biocompatibility of EVs [41, 42]. After 7 h of co-incubation, lysosomes and siRNA were co-localized in the EVs@UiO-66-NH_2@FAM-siRNA group (indicated by yellow fluorescence), indicating that a large amount of siRNA from nanoparticles had entered the lysosomes. By 12 h, a significant amount of green fluorescence was observed in the EVs@UiO-66-NH_2@FAM-siRNA group, suggesting that the acid-dependent skeletal structure of nanoparticles began to degrade in the acidic environment of lysosomes, allowing siRNA to effectively escape into the cytoplasm [43]. By contrast, due to its poor biocompatibility, only a small amount of siRNA was found to enter the cells in the UiO-66-NH_2@FAM-siRNA group. Flow cytometry revealed similar results: the fluorescence intensity of the EVs@UiO-66-NH_2@FAM-siRNA group was higher than that of the UiO-66-NH_2@FAM-siRNA group after co-incubation of nanoparticles with cells for 3 h, 7 h, and 12 h (Fig. 2E, F and Fig. S3 E, F). This indicates that UiO-66-NH_2 nanoparticles encapsulated with EVs enhances their cellular uptake [44].

Anti-inflammatory effects of EVs@UiO-66-NH_2@siRNA in vitro

Before assessing the anti-inflammatory effects of nanoparticles in RAW264.7 cells, we determined the safety of nanoparticles in vitro. Six types of nanoparticles (siRNA, UiO-66-NH_2, EVs, EVs@UiO-66-NH_2, UiO-66-NH_2@siRNA, EVs@UiO-66-NH_2@siRNA) were co-incubated with RAW264.7 and HT-29 cells for 24 h, and cell viability was assessed using the MTT assay. As shown in Fig. 3A, no impact on cell viability was observed during the entire 24 h co-incubation period of nanoparticles with RAW264.7 and HT-29 cells, indicating good safety (Fig. 3A and Fig. S4 A).

Macrophages, as primary inflammatory immune cells, play a crucial role in the initiation and progression of inflammation by secreting various cytokines under inflammatory stimuli [45, 46]. To evaluate whether our siRNA could effectively inhibit TNF-α production, cell culture supernatants were treated with nanoparticles alongside LPS to stimulate TNF-α production. Compared to cultures treated with LPS alone, cells treated with siRNA or UiO-66-NH_2 showed similar TNF-α induction, suggesting that free siRNA and empty UiO-66-NH_2 nanoparticles lack anti-inflammatory activity. By contrast, TNF-α concentrations were reduced in cells treated with EVs, EVs@UiO-66-NH_2, UiO-66-NH_2@siRNA, and EVs@UiO-66-NH_2@siRNA (Fig. 3B). Interestingly, EVs and EVs@UiO-66-NH_2 groups that do not contain siRNA reduced TNF-α levels by over 45%, suggesting a natural anti-inflammatory effect of EVs. Treatment of LPS-treated cells with UiO-66-NH_2@siRNA and EVs@UiO-66-NH_2@siRNA reduced TNF-α levels by 57% and 78%, respectively. Thus, the combination of gene silencing and a natural anti-inflammatory activity in the EVs@UiO-66-NH_2@siRNA group resulted in the most significant reduction in TNF-α concentration. Other inflammatory factors were also tested, revealing that EVs, EVs@UiO-66-NH_2, and EVs@UiO-66-NH_2@siRNA nanoparticles reduced the concentrations of inflammatory factors IL-6 and IL-1β to a similar extent, and increased the concentration of the anti-inflammatory factor IL-10 (Fig. 3C-E). Taken together, the results indicate that EVs derived from *Lactobacillus acidophilus* play a significant role in inflammation by increasing the levels of anti-inflammatory factors (such as IL-10) and decreasing the levels of pro-inflammatory factors (such as IL-6 and IL-1β). The addition of TNF-α siRNA further reduces the inflammatory response. The cytokine expression in HT-29 cells was also evaluated. The changes in cytokine levels were similar to those illustrated in Fig. 3B-E (Fig. S4 B-E), suggesting that EVs@UiO-66-NH_2@siRNA nanoparticles possess great ability in the regulation of inflammatory factors in intestinal epithelial cell.

Furthermore, the clinically relevant UC drug (EVs@UiO-66-NH_2@anti-TNF-α antibody) and commercial delivery system (Liposome@TNF-α siRNA) were also prepared and investigated. In terms of reducing TNF-α level in RAW264.7 cells, EVs@UiO-66-NH_2@siRNA exhibited better therapeutic effect then EVs@UiO-66-NH_2@anti-TNF-α antibody (Fig. S6 A). Meanwhile, EVs@UiO-66-NH_2@siRNA exhibited a stronger effect

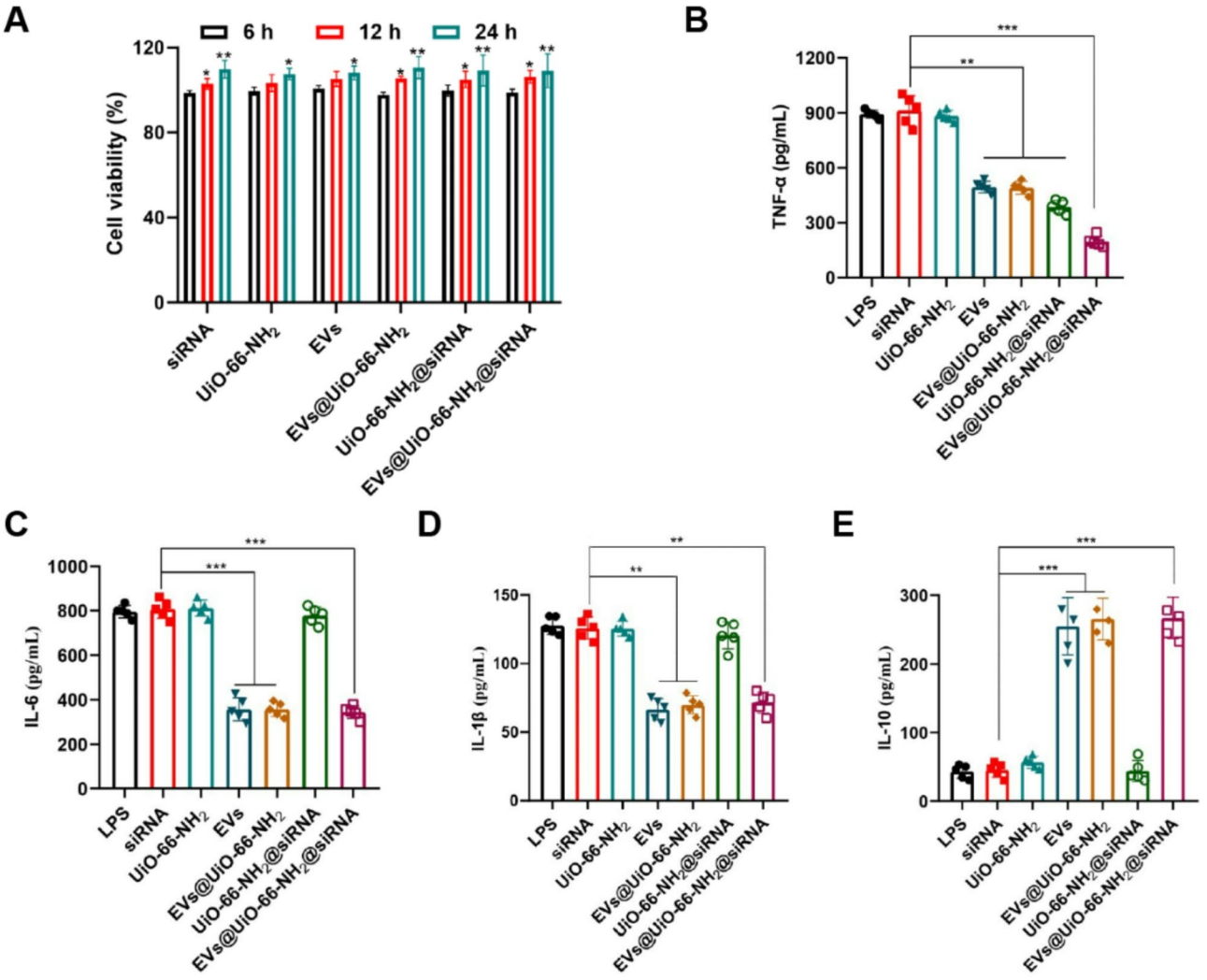

Fig. 3 Anti-inflammatory effects of EVs@UiO-66-NH_2@siRNA in vitro. (**A**) After treatment of RAW264.7 cells with siRNA, UiO-66-NH_2, EVs, EVs@UiO-66-NH_2, UiO-66-NH_2@siRNA, and EVs@UiO-66-NH_2@siRNA, cell viability was assessed using the MTT method ($n=5$). (**B**-**D**) Following treatment with different nanoparticles, the levels of TNF-α, IL-6, IL-1β, and IL-10 in cells were measured using ELISA ($n=5$). Data are presented as mean ± SD. * $P<0.05$, ** $P<0.01$, *** $P<0.001$

than Liposome@TNF-α siRNA in reducing IL-6 and IL-1β levels and increasing IL-10. These results demonstrate the advantages of combination therapy of EVs@UiO-66-NH_2@siRNA over current systems.

Distribution of EVs@UiO-66-NH_2@siRNA in the Gastrointestinal tract

To observe the distribution of nanoparticles in the gastrointestinal tract after gavage, we used Cy5.5-labeled siRNA (Cy5.5-siRNA) and performed quantitative analysis of the fluorescence signal in colon tissue 24 h post-administration (Fig. 4A and C). The results indicated that throughout the entire testing period, free Cy5.5-siRNA exhibited overall weak fluorescence signals in the gastrointestinal tract, suggesting rapid degradation of free Cy5.5-siRNA in the absence of EV membrane and UiO-66-NH_2 protection. Compared to the free Cy5.5-siRNA group, an increase in fluorescence intensity was observed in the UiO-66-NH_2@Cy5.5-siRNA group; however, the fluorescence signal observed in colon tissue was limited, indicating that while UiO-66-NH_2 can provide transient protection for Cy5.5-siRNA, the lack of targeting ability results in minimal siRNA entering colon tissue. This limited fluorescence signal may be attributed to the enhanced permeability and retention effect (EPR) effect of UiO-66-NH_2 nanoparticles [47, 48]. By contrast, the EVs@UiO-66-NH_2@Cy5.5-siRNA group showed a significant accumulation of fluorescence signal in colon tissue after 24 h. This demonstrated that EVs enhanced the targeting ability of nanoparticles allowing EVs@UiO-66-NH_2@Cy5.5-siRNA quickly navigate the harsh acidic environment in the gastrointestinal tract to reach

the colon successfully. Within 24 h post-gavage, fluorescence signals in other major organs (heart, liver, spleen, lungs, kidneys) were negligible, indicating that EVs@UiO-66-NH_2@Cy5.5-siRNA primarily undergo metabolism in the gastrointestinal tract post-gavage (Fig. 4B). In summary, the results of in vivo fluorescence distribution demonstrate that EVs@UiO-66-NH_2@Cy5.5-siRNA possess robust colon-targeting and accumulation.

In vivo anti-inflammatory effect of EVs@UiO-66-NH_2@siRNA

Colonic inflammation induced by DSS is one of the most commonly used animal models to simulate UC [49]. After DSS administration for 7 days, we evaluated the therapeutic effect of treatment with EVs@UiO-66-NH_2@siRNA for 4 days (Fig. 5A). Various parameters related to mouse inflammation were meticulously recorded throughout the study period, including body weight as an overall measure of health. Compared to the healthy control group, mice treated with DSS exhibited a significant overall decrease in body weight during the DSS treatment period, and continued to lose weight after treatment with siRNA and UiO-66-NH_2. After treatment with EVs, EVs@UiO-66-NH_2, UiO-66-NH_2@siRNA, and EVs@UiO-66-NH_2@siRNA, the rate of body weight loss was lessened than the free siRNA and UiO-66-NH_2. For

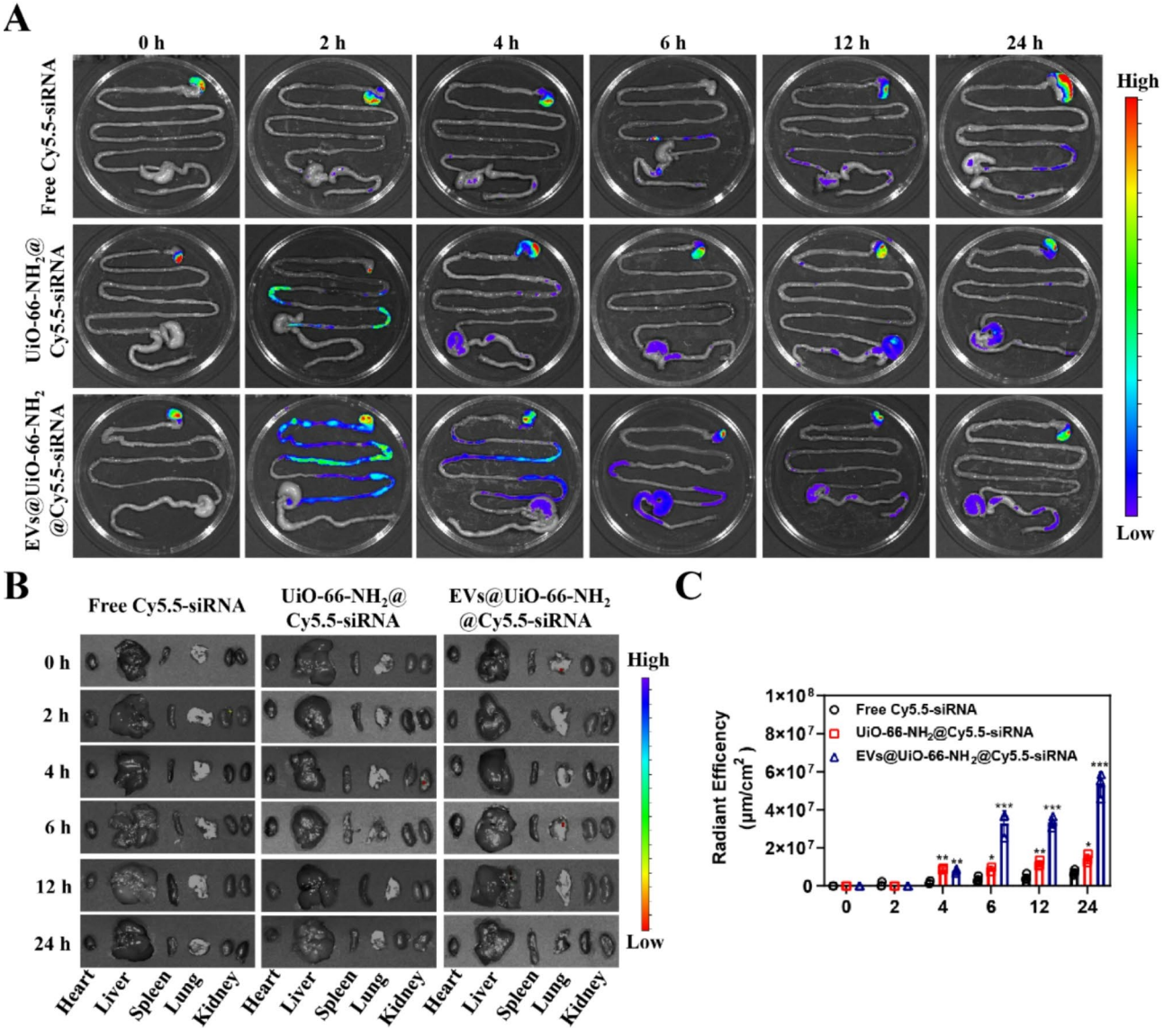

Fig. 4 Distribution of EVs@UiO-66-NH_2@siRNA in the gastrointestinal tract. (**A**) Distribution of free Cy5.5-siRNA, UiO-66-NH_2@Cy5.5-siRNA, and EVs@UiO-66-NH_2@Cy5.5-siRNA, in the gastrointestinal tract of mice 24 h following oral administration. (**B**) Distribution of the three types of nanoparticles in other major organs (heart, liver, spleen, lung, kidney). (**C**) Quantitative analysis of Cy5.5 fluorescence signals in colon tissues after oral administration of the three types of nanoparticles for 24 h ($n = 3$). Data are presented as means ± SD. * $P < 0.05$, ** $P < 0.01$, *** $P < 0.001$

EVs and EVs@UiO-66-NH_2 groups, this effect was attributed to the natural anti-inflammatory activity of *Lactobacillus* EVs, while in the UiO-66-NH_2@siRNA group, it may be attributed to the silencing effect of TNF-α siRNA. In contrast to all other experimental groups, only the EVs@UiO-66-NH_2@siRNA group showed body weight gain, effective immediately upon treatment (Fig. 5B). This suggests that the combined silencing effect of TNF-α siRNA together with the natural anti-inflammatory activity of EVs led to the optimal recovery of body weight in DSS mice.

The Disease Activity Index (DAI) quantifies the severity of UC by scoring weight loss, stool consistency, and rectal bleeding [50]. As expected, the DAI of healthy mice was near 0 and remained stable during the study, whereas the DAI increased rapidly in DSS-treated mice. On the 12th day, DAI values decreased after treatment with EVs, EVs@UiO-66-NH_2, and UiO-66-NH_2@siRNA as compared to free siRNA and UiO-66-NH_2. The most significant decrease was observed for EVs@UiO-66-NH_2@siRNA treatment, indicating a therapeutic effect in reducing the severity of colitis (Fig. 5C).

Colon length is a direct indicator of the degree of inflammation induced by DSS in UC [51]. As seen in Fig. 5D and E, compared to healthy control mice, DSS mice treated with free siRNA and UiO-66-NH_2 exhibited a 51.4% decrease in colon length, while mice treated with EVs and EVs@UiO-66-NH_2 showed a 39.1% decrease, UiO-66-NH_2@siRNA-treated mice showed a 37.7% decrease, and mice treated with EVs@UiO-66-NH_2@siRNA showed only a 19.9% decrease (Fig. 5D and E). These results indicate that EVs@UiO-66-NH_2@siRNA had the best therapeutic effect among all groups. Treatment with DSS also caused an increase in spleen weight, which is typically associated with the severity of inflammation and anemia [52]. However, treatment with EVs@UiO-66-NH_2@siRNA alleviated splenomegaly in DSS-induced UC mice (Fig. 5F and G).

Dysregulated immune responses are closely associated with the development of UC [53]. Therefore, the activity of myeloperoxidase (MPO), a crucial indicator of neutrophil infiltration and inflammation, in colonic tissues was assessed [54]. After one day of treatment, the MPO concentration in colon tissue remained largely unchanged in different groups (Fig. S5 A). After five days of treatment with EVs, EVs@UiO-66-NH_2, UiO-66-NH_2@siRNA, and EVs@UiO-66-NH_2@siRNA, the concentration of MPO in colonic tissues decreased, indicating a reduced inflammation was achieved (Fig. S7). The MPO activity in the EVs@UiO-66-NH_2@siRNA group was particularly lower than other groups, suggesting that EVs@UiO-66-NH_2@siRNA effectively alleviates intestinal inflammation. Cytokine mRNA levels (TNF-α, IL-6, IL-1β, IL-10) in colonic tissues were detected using qRT-PCR. The expression of mRNA levels of inflammatory factors remained unchanged after one day treatment: TNF-α, IL-6 and IL-1β showed highly expressed, and IL-10 mRNA expression was low (Fig. S5 B-E), which was caused by the insufficient treatment efficacy at early stage. At the end of the treatment, high expression of TNF-α mRNA was observed in the free siRNA and UiO-66-NH_2 groups, but after treatment with EVs, EVs@UiO-66-NH_2, UiO-66-NH_2@siRNA, and EVs@UiO-66-NH_2@siRNA, TNF-α mRNA levels decreased, with the greatest decrease observed in the EVs@UiO-66-NH_2@siRNA group (Fig. 5H). This indicates that UiO-66-NH_2 loaded with TNF-α siRNA can synergistically reduce TNF-α mRNA levels in conjunction with *Lactobacillus acidophilus* EVs. After treatment with EVs, EVs@UiO-66-NH_2, and EVs@UiO-66-NH_2@siRNA, similar decreases in mRNA levels of pro-inflammatory cytokines IL-6 and IL-1β were observed, while expression of the anti-inflammatory cytokine IL-10 generally increased (Fig. 5I-K). The concentrations of cytokines in colon tissue were measured using the ELISA method, and the results were consistent with those obtained from cytokine mRNA detection (Fig. S5 F-I and Fig. 5L-O). EVs, EVs@UiO-66-NH_2 and EVs@UiO-66-NH_2@siRNA had similar regulatory effects on the expressions of IL-6, IL-1β and IL-10, which attributed to the inherent anti-inflammatory activity of EVs. Additionally, the incorporation of TNF-α siRNA in EVs@UiO-66-NH_2@siRNA led to an obvious decrease in the expressions of TNF-α. H&E staining revealed that after treatment with EVs@UiO-66-NH_2@siRNA, the intestinal epithelium and crypt structures of DSS-induced mice became regular and intact, indicating intestinal repair (Fig. 5P). In conclusion, by combining the anti-inflammatory activity of *Lactobacillus acidophilus* EVs with the gene silencing effect of TNF-α siRNA, a synergistic therapeutic effect can be exerted in DSS-induced UC.

Regulation of gut microbiota and metabolites by EVs@UiO-66-NH_2@siRNA

An increasing number of studies have indicated that gut microbiota play a crucial role in the progression of UC [55, 56]. Particularly, alterations in the composition of metabolites induced by changes in gut microbiota have been shown to play an important role in gut immunoregulation and epithelial cell repair [57]. Encouraged by the satisfactory therapeutic effects of EVs@UiO-66-NH_2@siRNA shown in the previous section, we further investigated whether EVs@UiO-66-NH_2@siRNA treatment could modulate the dysbiosis of gut microbiota and metabolite composition in UC mice. Initially, we conducted 16 S rRNA gene sequencing on fecal samples from healthy mice, DSS-induced mice, and DSS-induced mice treated with EVs@UiO-66-NH_2@siRNA.

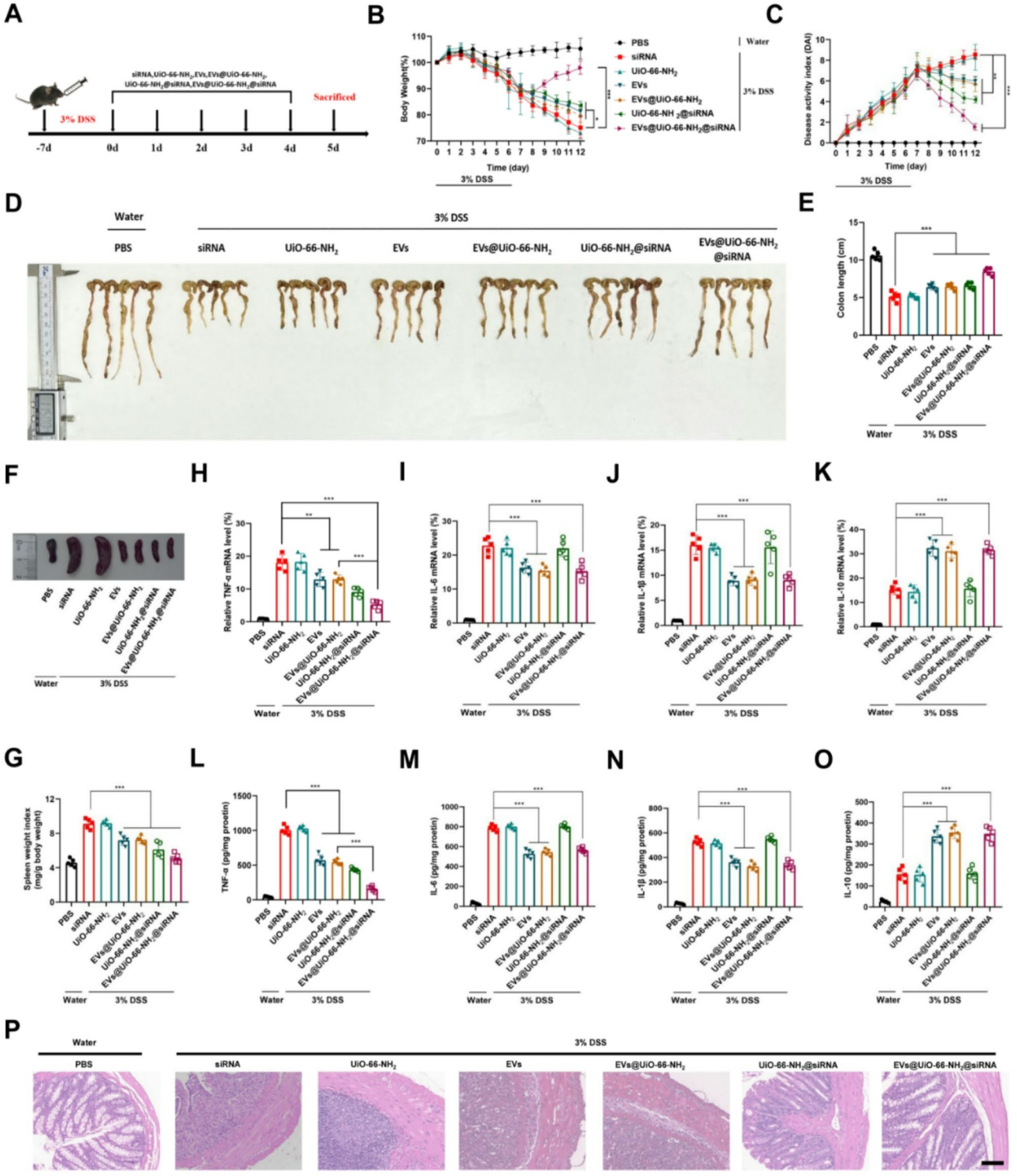

Fig. 5 Anti-inflammatory effects of EVs@UiO-66-NH_2@siRNA in vivo. (**A**) Schematic representation of the experimental design. (**B**) Changes in body weight of each group of mice over 13 days ($n = 5$). (**C**) Changes in disease activity index of each group of mice over 13 days ($n = 5$). (**D**) Images of colon tissues. (**E**) Statistical analysis of colon lengths ($n = 5$). (**F**) Representative images of spleens. (**G**) Changes in spleen index ($n = 5$). (**H**-**K**) Quantitative RT-PCR analysis of relative mRNA expression levels of TNF-α, IL-6, IL-1β, and IL-10 in colon tissues ($n = 5$). (**L**-**O**) ELISA detection of TNF-α, IL-6, IL-1β, and IL-10 levels in colon tissues ($n = 5$). (**P**) Representative H&E-stained images of colon tissues at the end of treatment (scale bar = 20 μm). Data were presented as mean ± SD. * $P < 0.05$, ** $P < 0.01$, *** $P < 0.001$

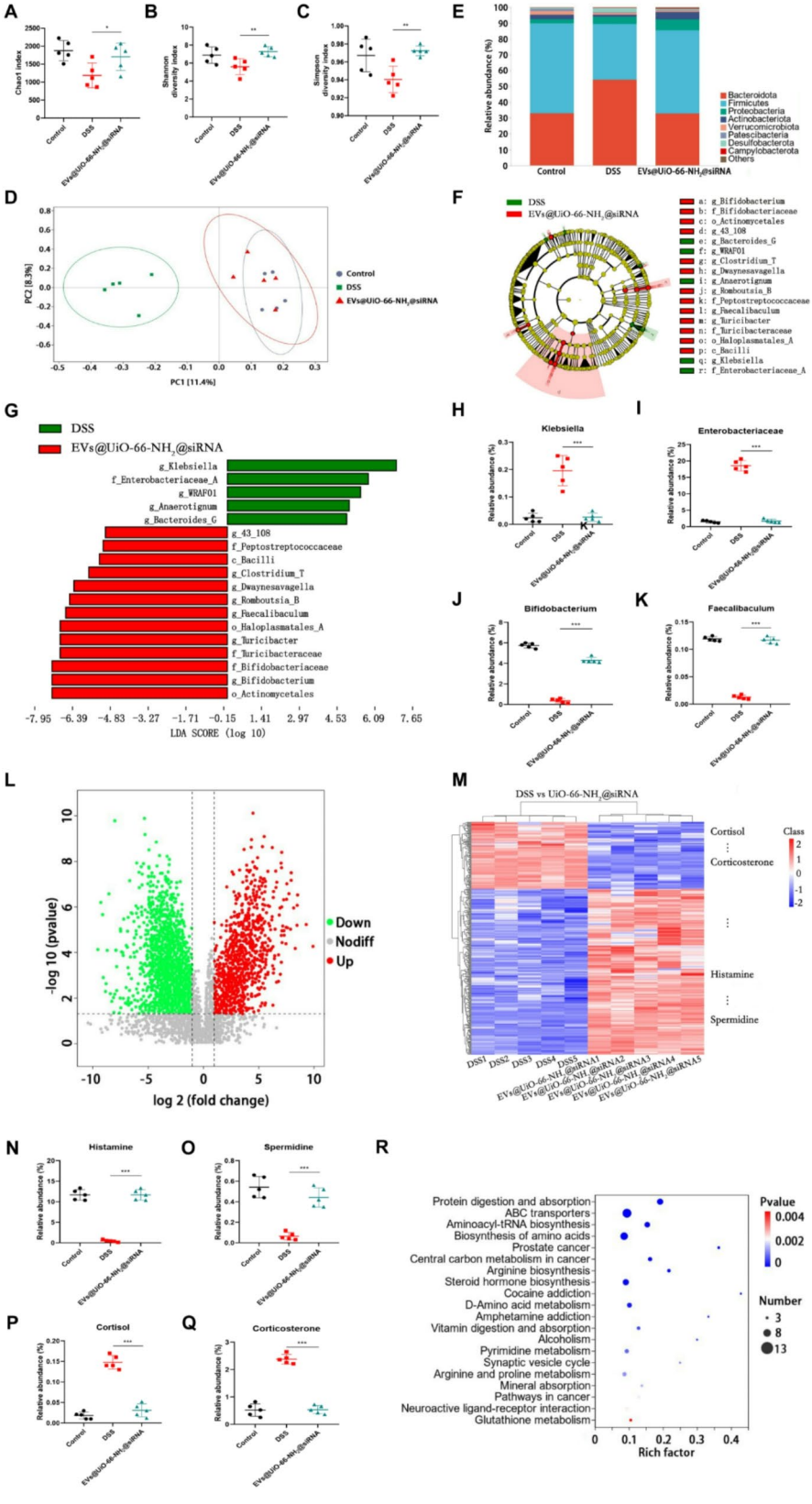

Fig. 6 (See legend on next page.)

(See figure on previous page.)

Fig. 6 Regulation of gut microbiota and metabolite by EVs@UiO-66-NH_2@siRNA. Comparison of microbial α-diversity assessed by (**A**) Chao1 index, (**B**) Shannon index and (**C**) Simpson index. (**D**) Principal component (PC) analysis plot illustrating the diversity of microbiota. (**E**) Column diagram of the relative abundance of gut microbiome at the phylum level. (**F**) Linear discriminant analysis effect (LEfSe) size illustrating differences in gut microbiota taxa for the DSS group versus the EVs@UiO-66-NH_2@siRNA group. (**G**) Distribution histogram based on linear discriminant analysis (LDA). LDA (log10) > 3.0. (**H**-**I**) The relative abundance of changes in representative bacterial taxa (**H**) *Klebsiella*, (**I**) *Enterobacteriaceae*, (**J**) *Bifidobacterium* and (**K**) *Faecalibaculum*. (**L**) Volcano plot of the differential metabolites, wherein each point represents a metabolite. Significantly up-regulated metabolites are indicated by red points and significantly down-regulated metabolites are indicated by green points and no difference metabolites are indicated by gray points. (**M**) Heat map of the differential metabolite clustering in the DSS group and EVs@UiO-66-NH_2@siRNA group. (**N**-**Q**) The relative abundance of changes in representative differential metabolite (**N**) histamine, (**O**) spermidine, (**P**) cortisol and (**Q**) corticosterone. (**R**) KEGG enrichment plot of the differential metabolites in the DSS group and EVs@UiO-66-NH_2@siRNA group. Data are presented as mean ± SD. * $P < 0.05$, ** $P < 0.01$, *** $P < 0.001$

Analysis of microbial α-diversity indicated a decrease in the Chao1 index, Shannon index, Simpson index, and number of observed species index in DSS-treated UC mice, which is consistent with the commonly reported decrease in microbial diversity and community richness accompanying DSS-induced UC [58]. By contrast, treatment with EVs@UiO-66-NH_2@siRNA caused an increase in these indices and a return to levels similar to those of healthy mice (Fig. 6A-C and Fig. S8). This suggests that EVs@UiO-66-NH_2@siRNA can improve microbial diversity and community richness in UC mice. We then analyzed differences in microbial community composition among treatment groups based on microbial β-diversity. Principal coordinate analysis (PCoA) showed that the gut microbiota of mice treated with EVs@UiO-66-NH_2@siRNA clustered closely with that of healthy mice and had no overlap with the DSS group (Fig. 6D), indicating that EVs@UiO-66-NH_2@siRNA can restore the gut microbiota of UC mice to a healthy state. The UniFrac distance matrix without weighting was used for UPGMA cluster analysis in this study, and the clustering results were combined with the relative species abundance of each sample at the phylum and genus levels. At the phylum level, clustering analysis showed changes in the relative abundance of 8 phyla representing gut microbiota. Specifically, in the DSS group, a decrease in the abundance of *Firmicutes* and an increase in *Bacteroidetes* were observed. After treatment with EVs@UiO-66-NH_2@siRNA, the abundance of *Firmicutes* increased while the abundance of *Bacteroidetes* decreased, resulting in an increase in the *Firmicutes*/*Bacteroidetes* (F/B) ratio post-treatment (Fig. 6E and Fig. S9). Previous reports have demonstrated an impact of the F/B ratio on microbial homeostasis in the gut, with UC typically associated with a decreased F/B ratio [59]. At the genus level, clustering analysis revealed changes in the abundance of 10 genera representing the gut microbiota. A decrease in *Escherichia* (a typical gut pathogen [60]) and an increase in probiotic genera such as *Lactobacillus*, *Bifidobacterium*, and *Limosilactobacillus* were observed in the EVs@UiO-66-NH_2@siRNA group (Fig. S10) [61–63]. Taken together, clustering analysis at the phylum and genus levels suggest that EVs@UiO-66-NH_2@siRNA has the potential to restore the microbiota of UC mice to a healthy state. Using Linear Discriminant Analysis Effect Size (LEfSe), microbial community differences between the DSS group and the EVs@UiO-66-NH_2 group were compared, and statistical analyses were performed on several representative families and genera. The results indicated that treatment with EVs@UiO-66-NH_2@siRNA reduced the abundance of *Klebsiella* (known to be abundant in patients with pathogenic colitis [64]) and *Enterobacteriaceae* (a group of Gram-negative rods residing in the gut, mostly commensals with a few pathogens [65]), while increasing the abundance of gut probiotics such as *Bifidobacterium* and *Faecalibaculum* (Fig. 6F-K [66]). In summary, these findings provide ample evidence that EVs@UiO-66-NH_2@siRNA can modulate the gut microbiota, increasing their abundance and diversity and aiding in the treatment of UC in mice.

Several studies have indicated that metabolites produced by microorganisms influence colonic immune homeostasis and mucosal integrity [67, 68]. To investigate the impact of metabolites on the treatment of UC, an untargeted metabolomics analysis was conducted on the fecal metabolite profiles of healthy mice, DSS-induced colitis mice, and DSS-induced colitis mice treated with EVs@UiO-66-NH_2@siRNA. Volcano plots revealed significant changes in the metabolites of mice treated with EVs@UiO-66-NH_2@siRNA compared to the untreated DSS group (Fig. 6L). Specifically, heatmap clustering of differential metabolites revealed that compared to the DSS group, histamine and spermidine increased while cortisol and corticosterone decreased in the EVs@UiO-66-NH_2@siRNA group (Fig. 6M-Q). Histamine and spermidine are reported to have anti-inflammatory effects: histamine can inhibit the production of pro-inflammatory cytokines by macrophages, suppress the activation of NF-κB, and thereby impede the progression of UC [69]. Spermidine can maintain normal gut microbiota by inhibiting the expression of α-defensins in colonic epithelial cells [70]. Cortisol and corticosterone, elevated in colitis mice, are believed to promote inflammation [71, 72]. Differential metabolite KEGG enrichment analysis illustrated that EVs@UiO-66-NH_2@siRNA selectively inhibited and promoted the presence of gut microbiota species, leading to alterations in metabolite composition (Fig. 6R). In conclusion, these findings suggest that

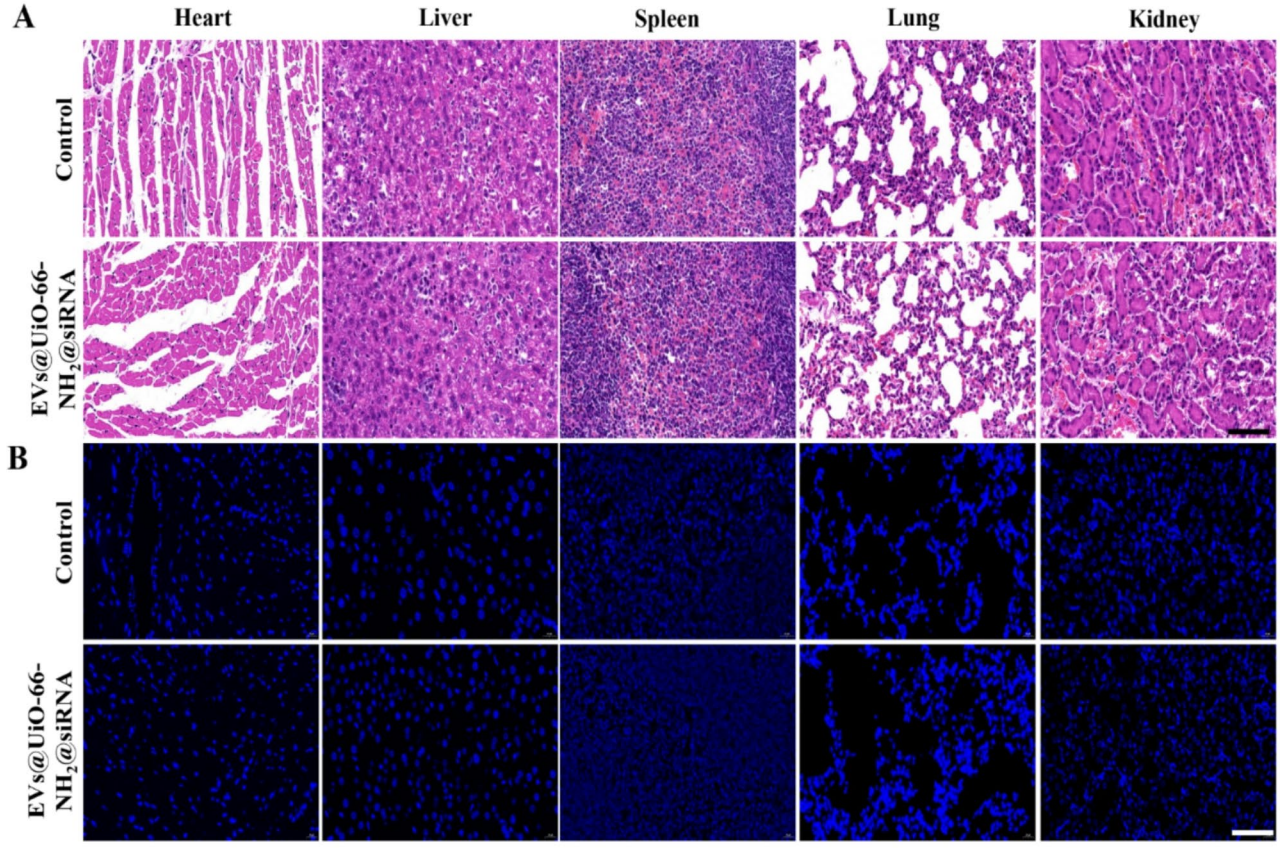

Fig. 7 Biocompatibility study of EVs@UiO-66-NH_2@siRNA. (**A**) Representative H&E staining of major organs and (**B**) TUNEL fluorescence staining. Scale bar = 20 μm

treatment with EVs@UiO-66-NH_2@siRNA can modulate gut microbiota and metabolite composition in DSS-induced colitis mice, generate the anti-inflammatory compounds histamine and spermidine, regulate immunity, and promote the proliferation and differentiation of colonic epithelial cells altogether, alleviating intestinal inflammation.

Biocompatibility of EVs@UiO-66-NH_2@siRNA

Finally, to investigate the potential toxicity of EVs@UiO-66-NH_2@FAM-siRNA in vivo, high doses of EVs@UiO-66-NH_2@FAM-siRNA were orally administered to healthy mice. Blood samples were collected from the mice after 24 h, along with important organs. Hematoxylin and eosin (H&E) staining revealed that compared to the healthy group of mice, there were no morphological changes observed in the overall structure and integrity of the heart, liver, spleen, lungs, and kidneys in mice treated with high doses of EVs@UiO-66-NH_2@FAM-siRNA (Fig. 7A). Terminal deoxynucleotidyl transferase-mediated dUTP-biotin nick end labeling assay (TUNEL) staining results indicated that the level of cell apoptosis in vital organs of the nanoparticle-treated group was similar to that of healthy mice (Fig. 7B). AST and ALT are two key liver enzymes that primarily used to assess liver function and detect liver damage [73]. As shown in Fig. S11 A and S11B, there were no significant differences in serum AST and ALT levels between EVs@UiO-66-NH_2@siRNA group and healthy group, indicating that the nanoparticles do not cause liver damage and affect hepatic function in mice. These results suggest that EVs@UiO-66-NH_2@FAM-siRNA exhibits good biocompatibility and can serve as a safe siRNA delivery vehicle for the treatment of UC.

Conclusions

In summary, we have developed a *Lactobacillus acidophilus* EVs-coated UiO-66-NH_2 delivery system that can effectively deliver TNF-α siRNA for the treatment of UC. UiO-66-NH_2 nanoparticles exhibit high siRNA loading capacity and favorable degradation, which improve the effectively release of siRNA within cell lysosomes and the cell uptake. In vitro experiments also demonstrate that *Lactobacillus acidophilus* EVs coating show potent anti-inflammatory capabilities in regulating the levels of pro-inflammatory cytokines of IL-6, and IL-1β, IL-10. After oral administration, specific colonic targeting of *Lactobacillus acidophilus* EVs ensures the accurate and

efficient delivery of EVs@UiO-66-NH_2@siRNA to colonic tissues, where siRNA can silence the TNF-α expression and exert a combined therapeutic effect. Moreover, beneficial changes are occurred in the gut microbiota of UC mice, with an increase in the abundance of probiotic strains such as *Bifidobacterium* and *Faecalibaculum*, and a decrease in pathogenic bacteria such as *Escherichia* and *Klebsiella*, which helps to maintain gut microbiota homeostasis. These alterations in the gut microbiota also lead to changes in metabolite profiles, which effectively regulate gut immunity and promote intestinal barrier repair, highlighting the comprehensive therapeutic effect of this system. In conclusion, this nano-delivery system provides a more precise strategy for UC treatment without off-target side effects, which may also appropriate for other gastrointestinal diseases like Crohn's disease. By restoring immune balance and alleviating chronic inflammation and improving dysbiosis, this approach provides potential for developing personalized therapeutics and broadens new horizons for disease treatment.

Supplementary Information

The online version contains supplementary material available at https://doi.org/10.1186/s12951-025-03376-0.

Supplementary Material 1

Acknowledgements
This work was supported by the National Natural Science Foundation of China (No. 82402437) and the Key Research and Development Special Fund of Henan Province (No. 231111311800, 252102311094). The authors are also grateful to the supports from Center of Advanced Analysis & Gene Sequencing of Zhengzhou University.

Author contributions
H.B.W, Z.W.S and C.Y.C conceived and designed the experiments. C.Y.C and J.Z.T performed most of the experiments. C.Y.C and J.C, B.J.Z and R.N.L prepared and characterized EVs@UiO-66-NH2 nanoparticles. Q.Z and C.J.Q provided assistance in the in vitro cell assay. R.C.C and G.M lent support in the in vivo animal experiment. C.Y.C wrote the manuscript. H.B.W and Z.W.S supported this study and approved the final version of the manuscript.

Data availability
No datasets were generated or analysed during the current study.

Declarations

Ethics approval and consent to participate
All animal experiments were conducted under the Regional Ethics Committee for Animal Experiments at Zhengzhou University.

Competing interests
The authors declare no competing interests.

Received: 26 December 2024 / Accepted: 6 April 2025
Published online: 17 April 2025

References

1. Gros B, Kaplan GG. Ulcerative colitis in adults: A review. JAMA. 2023;330:951–65.
2. Adams A, Gupta V, Mohsen W, Chapman TP, Subhaharan D, Kakkadasam Ramaswamy P, Kumar S, Kedia S, McGregor CG, Ambrose T, et al. Early management of acute severe UC in the biologics era: development and international validation of a prognostic clinical index to predict steroid response. Gut. 2023;72:433–42.
3. Franzosa EA, Sirota-Madi A, Avila-Pacheco J, Fornelos N, Haiser HJ, Reinker S, Vatanen T, Hall AB, Mallick H, McIver LJ, et al. Gut Microbiome structure and metabolic activity in inflammatory bowel disease. Nat Microbiol. 2019;4:293–305.
4. Chen Y, Mai Q, Chen Z, Lin T, Cai Y, Han J, Wang Y, Zhang M, Tan S, Wu Z, et al. Dietary palmitoleic acid reprograms gut microbiota and improves biological therapy against colitis. Gut Microbes. 2023;15:2211501.
5. Yang W, Cong Y. Gut microbiota-derived metabolites in the regulation of host immune responses and immune-related inflammatory diseases. Cell Mol Immunol. 2021;18:866–77.
6. Yuan X, Chen B, Duan Z, Xia Z, Ding Y, Chen T, Liu H, Wang B, Yang B, Wang X, et al. Depression and anxiety in patients with active ulcerative colitis: crosstalk of gut microbiota, metabolomics and proteomics. Gut Microbes. 2021;13:1987779.
7. Li N, Ma P, Li Y, Shang X, Nan X, Shi L, Han X, Liu J, Hong Y, Li Q, et al. Gut microbiota-derived 12-ketolithocholic acid suppresses the IL-17A secretion from colonic group 3 innate lymphoid cells to prevent the acute exacerbation of ulcerative colitis. Gut Microbes. 2023;15:2290315.
8. Yang W, Wang Y, Tao K, Li R. Metabolite Itaconate in host immunoregulation and defense. Cell Mol Biol Lett. 2023;28:100.
9. Yang J, Pei G, Sun X, Xiao Y, Miao C, Zhou L, Wang B, Yang L, Yu M, Zhang ZS, et al. RhoB affects colitis through modulating cell signaling and intestinal Microbiome. Microbiome. 2022;10:149.
10. Liu L, Wang H, Chen X, Zhang Y, Zhang H, Xie P. Gut microbiota and its metabolites in depression: from pathogenesis to treatment. EBioMedicine. 2023;90:104527.
11. Wang MX, Lin L, Chen YD, Zhong YP, Lin YX, Li P, Tian X, Han B, Xie ZY, Liao QF. Evodiamine has therapeutic efficacy in ulcerative colitis by increasing Lactobacillus acidophilus levels and acetate production. Pharmacol Res. 2020;159:104978.
12. Li P, Chen G, Zhang J, Pei C, Chen Y, Gong J, Deng S, Cai K, Li H, Wang D, et al. Live Lactobacillus acidophilus alleviates ulcerative colitis via the SCFAs/mitophagy/NLRP3 inflammasome axis. Food Funct. 2022;13:2985–97.
13. Barros de Medeiros VP, Salgaço MK, Pimentel TC, Rodrigues da Silva TC, Sartoratto A, Lima MDS, Sassi C, Mesa V, Magnani M, Sivieri K. Spirulina platensis biomass enhances the proliferation rate of Lactobacillus acidophilus 5 (La-5) and combined with La-5 impact the gut microbiota of medium-age healthy individuals through an in vitro gut Microbiome model. Food Res Int. 2022;154:110880.
14. Shi J, Xie Q, Yue Y, Chen Q, Zhao L, Evivie SE, Li B, Huo G. Gut microbiota modulation and anti-inflammatory properties of mixed lactobacilli in dextran sodium sulfate-induced colitis in mice. Food Funct. 2021;12:5130–43.
15. Zhou JS, Gopal PK, Gill HS. Potential probiotic lactic acid bacteria Lactobacillus rhamnosus (HN001), Lactobacillus acidophilus (HN017) and bifidobacterium lactis (HN019) do not degrade gastric mucin in vitro. Int J Food Microbiol. 2001;63:81–90.
16. Yun B, Oh S, Griffiths MW. Lactobacillus acidophilus modulates the virulence of clostridium difficile. J Dairy Sci. 2014;97:4745–58.
17. Li H, Shi J, Zhao L, Guan J, Liu F, Huo G, Li B. Lactobacillus plantarum KLDS1.0344 and Lactobacillus acidophilus KLDS1.0901 mixture prevents chronic alcoholic liver injury in mice by protecting the intestinal barrier and regulating gut microbiota and liver-Related pathways. J Agric Food Chem. 2021;69:183–97.
18. Buzas EI. The roles of extracellular vesicles in the immune system. Nat Rev Immunol. 2023;23:236–50.
19. Boland BS, Boyle DL, Sandborn WJ, Firestein GS, Levesque BG, Hillman J, Zhang B, Proudfoot J, Eckmann L, Ernst PB, et al. Validated gene expression biomarker analysis for biopsy-based clinical trials in ulcerative colitis. Aliment Pharmacol Ther. 2014;40:477–85.
20. Dong Y, Siegwart DJ, Anderson DG. Strategies, design, and chemistry in SiRNA delivery systems. Adv Drug Deliv Rev. 2019;144:133–47.
21. Anthiya S, Öztürk SC, Yanik H, Tavukcuoglu E, Şahin A, Datta D, Charisse K, Álvarez DM, Loza MI, Calvo A, et al. Targeted SiRNA lipid nanoparticles for the treatment of KRAS-mutant tumors. J Control Release. 2023;357:67–83.
22. Ball RL, Hajj KA, Vizelman J, Bajaj P, Whitehead KA. Lipid nanoparticle formulations for enhanced Co-delivery of SiRNA and mRNA. Nano Lett. 2018;18:3814–22.

23. Yadav K, Sahu KK, Sucheta, Gnanakani SPE, Sure P, Vijayalakshmi R, Sundar VD, Sharma V, Antil R, Jha M, et al. Biomedical applications of nanomaterials in the advancement of nucleic acid therapy: mechanistic challenges, delivery strategies, and therapeutic applications. Int J Biol Macromol. 2023;241:124582.
24. Gao M, Yang C, Wu C, Chen Y, Zhuang H, Wang J, Cao Z. Hydrogel-metal-organic-framework hybrids mediated efficient oral delivery of SiRNA for the treatment of ulcerative colitis. J Nanobiotechnol. 2022;20:404.
25. Xiao B, Chen Q, Zhang Z, Wang L, Kang Y, Denning T, Merlin D. TNFα gene Silencing mediated by orally targeted nanoparticles combined with interleukin-22 for synergistic combination therapy of ulcerative colitis. J Control Release. 2018;287:235–46.
26. Zhang G, Fan H, Zhou RY, Yin W, Wang R, Yang M, Xue Z, Yang Y, Yu JX. Decorating UiO-66-NH(2) crystals on recyclable fiber bearing polyamine and Amidoxime bifunctional groups via cross-linking method with good stability for highly efficient capture of U(VI) from aqueous solution. J Hazard Mater. 2022;424:127273.
27. Huo D, Zhang Y, Li N, Ma W, Liu H, Xu G, Li Z, Yang M, Hou C. Three-dimensional graphene/amino-functionalized metal-organic framework for simultaneous electrochemical detection of Cd(II), Pb(II), Cu(II), and Hg(II). Anal Bioanal Chem. 2022;414:1575–86.
28. Li X, Luo Y, Huang Z, Wang Y, Wu J, Zhou S. Multifunctional liposomes remodeling tumor immune microenvironment for tumor chemoimmunotherapy. Small Methods. 2023;7:e2201327.
29. Peterson GW, Mahle JJ, DeCoste JB, Gordon WO, Rossin JA. Extraordinary NO2 removal by the Metal-Organic framework UiO-66-NH2. Angew Chem Int Ed Engl. 2016;55:6235–8.
30. Jamshidifard S, Koushkbaghi S, Hosseini S, Rezaei S, Karamipour A, Jafari Rad A, Irani M. Incorporation of UiO-66-NH2 MOF into the PAN/chitosan nanofibers for adsorption and membrane filtration of Pb(II), Cd(II) and Cr(VI) ions from aqueous solutions. J Hazard Mater. 2019;368:10–20.
31. Yang L, Wang Z, Gong H, Gai S, Shen R. Tirapazamine-loaded UiO-66/Cu for ultrasound-mediated promotion of chemodynamic therapy cascade hypoxia-activated anticancer therapy. J Colloid Interface Sci. 2023;634:495–508.
32. Cui J, Zhang C, Liu H, Yang L, Liu X, Zhang J, Zhou Y, Zhang J, Yan X. Pulmonary delivery of Recombinant human bleomycin hydrolase using Mannose-Modified hierarchically porous UiO-66 for preventing bleomycin-Induced pulmonary fibrosis. ACS Appl Mater Interfaces. 2023;15:11520–35.
33. Yuan SN, Wang MX, Han JL, Feng CY, Wang M, Wang M, Sun JY, Li NY, Simal-Gandara J, Liu C. Improved colonic inflammation by nervonic acid via Inhibition of NF-κB signaling pathway of DSS-induced colitis mice. Phytomedicine. 2023;112:154702.
34. Moghadaskhou F, Tadjarodi A, Mollahosseini A, Maleki A. Synthesis of UiO-66-Sal-Cu(OH)(2) by a simple and novel method: MOF-Based metal thin film as a heterogeneous catalyst for olefin oxidation. ACS Appl Mater Interfaces. 2023;15:4021–32.
35. Oh JY, Choi E, Jana B, Go EM, Jin E, Jin S, Lee J, Bae JH, Yang G, Kwak SK, et al. Protein-Precoated surface of Metal-Organic framework nanoparticles for targeted delivery. Small. 2023;19:e2300218.
36. Wang Z, Fu Y, Kang Z, Liu X, Chen N, Wang Q, Tu Y, Wang L, Song S, Ling D, et al. Organelle-Specific triggered release of immunostimulatory oligonucleotides from intrinsically coordinated DNA-Metal-Organic frameworks with soluble exoskeleton. J Am Chem Soc. 2017;139:15784–91.
37. Bonnefoy J, Legrand A, Quadrelli EA, Canivet J, Farrusseng D. Enantiopure Peptide-Functionalized Metal-Organic frameworks. J Am Chem Soc. 2015;137:9409–16.
38. Ma P, Pan Y, Li W, Sun C, Liu J, Xu T, Shu Y. Extracellular vesicles-mediated noncoding RNAs transfer in cancer. J Hematol Oncol. 2017;10:57.
39. Liao FS, Lo WS, Hsu YS, Wu CC, Wang SC, Shieh FK, Morabito JV, Chou LY, Wu KC, Tsung CK. Shielding against unfolding by embedding enzymes in Metal-Organic frameworks via a de Novo approach. J Am Chem Soc. 2017;139:6530–3.
40. Zhang X, Zhang H, Gu J, Zhang J, Shi H, Qian H, Wang D, Xu W, Pan J, Santos HA. Engineered extracellular vesicles for cancer therapy. Adv Mater. 2021;33:e2005709.
41. Hade MD, Suire CN, Mossell J, Suo Z. Extracellular vesicles: emerging frontiers in wound healing. Med Res Rev. 2022;42:2102–25.
42. Cecchin R, Troyer Z, Witwer K, Morris KV. Extracellular vesicles: the next generation in gene therapy delivery. Mol Ther. 2023;31:1225–30.
43. Mantion A, Massüger L, Rabu P, Palivan C, McCusker LB, Taubert A. Metal-peptide frameworks (MPFs): bioinspired metal organic frameworks. J Am Chem Soc. 2008;130:2517–26.
44. Niu W, Xiao Q, Wang X, Zhu J, Li J, Liang X, Peng Y, Wu C, Lu R, Pan Y, et al. A biomimetic drug delivery system by integrating grapefruit extracellular vesicles and Doxorubicin-Loaded Heparin-Based nanoparticles for glioma therapy. Nano Lett. 2021;21:1484–92.
45. Fu B, Xiong Y, Sha Z, Xue W, Xu B, Tan S, Guo D, Lin F, Wang L, Ji J, et al. SEPTIN2 suppresses an IFN-γ-independent, Proinflammatory macrophage activation pathway. Nat Commun. 2023;14:7441.
46. Wynn TA, Vannella KM. Macrophages in tissue repair, regeneration, and fibrosis. Immunity. 2016;44:450–62.
47. Tian H, Zhang T, Qin S, Huang Z, Zhou L, Shi J, Nice EC, Xie N, Huang C, Shen Z. Enhancing the therapeutic efficacy of nanoparticles for cancer treatment using versatile targeted strategies. J Hematol Oncol. 2022;15:132.
48. Acharya S, Sahoo SK. PLGA nanoparticles containing various anticancer agents and tumour delivery by EPR effect. Adv Drug Deliv Rev. 2011;63:170–83.
49. Gao C, Zhou Y, Chen Z, Li H, Xiao Y, Hao W, Zhu Y, Vong CT, Farag MA, Wang Y, Wang S. Turmeric-derived nanovesicles as novel nanobiologics for targeted therapy of ulcerative colitis. Theranostics. 2022;12:5596–614.
50. Yao D, Dai W, Dong M, Dai C, Wu S. MUC2 and related bacterial factors: therapeutic targets for ulcerative colitis. EBioMedicine. 2021;74:103751.
51. Ma Y, Duan L, Sun J, Gou S, Chen F, Liang Y, Dai F, Xiao B. Oral nanotherapeutics based on antheraea pernyi silk fibroin for synergistic treatment of ulcerative colitis. Biomaterials. 2022;282:121410.
52. Yan YX, Shao MJ, Qi Q, Xu YS, Yang XQ, Zhu FH, He SJ, He PL, Feng CL, Wu YW, et al. Artemisinin analogue SM934 ameliorates DSS-induced mouse ulcerative colitis via suppressing neutrophils and macrophages. Acta Pharmacol Sin. 2018;39:1633–44.
53. Mitsialis V, Wall S, Liu P, Ordovas-Montanes J, Parmet T, Vukovic M, Spencer D, Field M, McCourt C, Toothaker J, et al. Single-Cell analyses of colon and blood reveal distinct immune cell signatures of ulcerative colitis and Crohn's disease. Gastroenterology. 2020;159:591–e608510.
54. Xiao Q, Li X, Li Y, Wu Z, Xu C, Chen Z, He W. Biological drug and drug delivery-mediated immunotherapy. Acta Pharm Sin B. 2021;11:941–60.
55. Nabavi-Rad A, Sadeghi A, Asadzadeh Aghdaei H, Yadegar A, Smith SM, Zali MR. The double-edged sword of probiotic supplementation on gut microbiota structure in Helicobacter pylori management. Gut Microbes. 2022;14:2108655.
56. Larabi A, Barnich N, Nguyen HTT. New insights into the interplay between autophagy, gut microbiota and inflammatory responses in IBD. Autophagy. 2020;16:38–51.
57. Adolph TE, Meyer M, Schwärzler J, Mayr L, Grabherr F, Tilg H. The metabolic nature of inflammatory bowel diseases. Nat Rev Gastroenterol Hepatol. 2022;19:753–67.
58. Lee Y, Sugihara K, Gillilland MG 3rd, Jon S, Kamada N, Moon JJ. Hyaluronic acid-bilirubin nanomedicine for targeted modulation of dysregulated intestinal barrier, Microbiome and immune responses in colitis. Nat Mater. 2020;19:118–26.
59. Yang W, Huang Z, Xiong H, Wang J, Zhang H, Guo F, Wang C, Sun Y. Rice protein peptides alleviate dextran sulfate Sodium-Induced colitis via the Keap1-Nrf2 signaling pathway and regulating gut microbiota. J Agric Food Chem. 2022;70:12469–83.
60. Tenaillon O, Skurnik D, Picard B, Denamur E. The population genetics of commensal Escherichia coli. Nat Rev Microbiol. 2010;8:207–17.
61. Khan H, Kadam A, Dutt D. Studies on bacterial cellulose produced by a novel strain of Lactobacillus genus. Carbohydr Polym. 2020;229:115513.
62. Laursen MF, Sakanaka M, von Burg N, Mörbe U, Andersen D, Moll JM, Pekmez CT, Rivollier A, Michaelsen KF, Mølgaard C, et al. Bifidobacterium species associated with breastfeeding produce aromatic lactic acids in the infant gut. Nat Microbiol. 2021;6:1367–82.
63. Wu Y, Ye Z, Feng P, Li R, Chen X, Tian X, Han R, Kakade A, Liu P, Li X. Limosilactobacillus fermentum JL-3 isolated from Jiangshui ameliorates hyperuricemia by degrading uric acid. Gut Microbes. 2021;13:1–18.
64. Schwabkey ZI, Wiesnoski DH, Chang CC, Tsai WB, Pham D, Ahmed SS, Hayase T, Ortega Turrubiates MR, El-Himri RK, Sanchez CA, et al. Diet-derived metabolites and mucus link the gut Microbiome to fever after cytotoxic cancer treatment. Sci Transl Med. 2022;14:eabo3445.
65. Nordmann P, Dortet L, Poirel L. Carbapenem resistance in enterobacteriaceae: here is the storm! Trends Mol Med. 2012;18:263–72.
66. Cao YG, Bae S, Villarreal J, Moy M, Chun E, Michaud M, Lang JK, Glickman JN, Lobel L, Garrett WS. Faecalibaculum rodentium remodels retinoic acid signaling to govern eosinophil-dependent intestinal epithelial homeostasis. Cell Host Microbe. 2022;30:1295–e13101298.

67. Schirmer M, Garner A, Vlamakis H, Xavier RJ. Microbial genes and pathways in inflammatory bowel disease. Nat Rev Microbiol. 2019;17:497–511.
68. Na YR, Stakenborg M, Seok SH, Matteoli G. Macrophages in intestinal inflammation and resolution: a potential therapeutic target in IBD. Nat Rev Gastroenterol Hepatol. 2019;16:531–43.
69. Andou A, Hisamatsu T, Okamoto S, Chinen H, Kamada N, Kobayashi T, Hashimoto M, Okutsu T, Shimbo K, Takeda T, et al. Dietary histidine ameliorates murine colitis by Inhibition of Proinflammatory cytokine production from macrophages. Gastroenterology. 2009;136:564–e574562.
70. Gobert AP, Latour YL, Asim M, Barry DP, Allaman MM, Finley JL, Smith TM, McNamara KM, Singh K, Sierra JC, et al. Protective role of spermidine in colitis and colon carcinogenesis. Gastroenterology. 2022;162:813–e827818.
71. Kojima K, Naruse Y, Iijima N, Wakabayashi N, Mitsufuji S, Ibata Y, Tanaka M. HPA-axis responses during experimental colitis in the rat. Am J Physiol Regul Integr Comp Physiol. 2002;282:R1348–1355.
72. Puppala ER, Aochenlar SL, Shantanu PA, Ahmed S, Jannu AK, Jala A, Yalamarthi SS, Borkar RM, Tripathi DM, Naidu VGM. Perillyl alcohol attenuates chronic restraint stress aggravated dextran sulfate sodium-induced ulcerative colitis by modulating TLR4/NF-κB and JAK2/STAT3 signaling pathways. Phytomedicine. 2022;106:154415.
73. Lv Q, Wang J, Yang H, Chen X, Zhang Y, Ji G, Hu L, Zhang Y. Didymin ameliorates ulcerative colitis-associated secondary liver damage by facilitating Notch1 degradation. Phytomedicine. 2024;134:155561.

Publisher's note